NASA CR-170429

TR-02-81

(NASA-CR-170429) UNBIASED ESTIMATION OF OCEANIC MEAN RAINFALL FROM SATELLITE BORNE RADIOMETER MEASUREMENTS (Engineering and Economics Research, Inc.) 63 p HC A04/MF A01 CSCL 04B G3/47

N82-32938

Unclas 33558

UNBIASED ESTIMATION OF OCEANIC MEAN RAINFALL FROM SATELLITE - BORNE RADIOMETER MEASUREMENTS

BY:

MAHESH C. MITTAL

PREPARED FOR:

NATIONAL AERONAUTICS AND SPACE ADMINISTRATION
GODDARD SPACE FLIGHT CENTER
GREENBELT, MARYLAND

ENGINEERING AND ECONOMICS RESEARCH, INC.
7700 LEESBURG PIKE
FALLS CHURCH, VIRGINIA 22043

APRIL 1981

ABSTRACT

The statistical properties of the radar derived rainfall obtained during the GARP Atlantic Tropical Experiment (GATE) are used to derive quantitative estimates of the spatial and temporal sampling errors associated with estimating rainfall from brightness temperature measurements such as would be obtained from a satellite-borne microwave radiometer employing a practical size antenna aperature. The analytic results of this study provide a basis for a method of correcting the so-called beam-filling problem: i.e., for the effect of non-uniformity of rainfall over the radiometer beamwidth. The method presented employs the statistical properties of the observations themselves without need for physical assumptions beyond those associated with the radiative transfer model. The simulation results presented offer a validation of the estimated accuracy that can be achieved and the graphs included permit evaluation of the effect of the antenna resolution on both the temporal and spatial sampling errors. For example, it is found that the bias associated with the antenna having a resolution of 32 km can be expected to be corrected to within ±6 percent of the monthly mean at a one sigma confidence level with two observations per day over a 256km x 256km region for which the GATE data can be considered typical.

TABLE OF CONTENTS

LIST OF FIGURES

LIST OF TABLES

1.0 INTRODUCTION

The Electronically Scanned Microwave Radiometer (ESMR) flown on the Nimbus-5 spacecraft demonstrated a capability to sense rainfall over ocean areas. The purpose of this study is to provide an increased understanding of the potential capabilities of microwave radiometry for remote observations of rainfall and to develop quantitative estimates and corresponding confidence bounds of the measurement accuracies that can be achieved. Results presented here should be of value in establishing the range of scientific requirements for remote observations of rainfall that can be met with current technology and they should be of further value in designing any future flight programs involving ESMR-like instruments.

The primary objectives of this study include:

1. Determination of the extent of bias errors due to non-uniform and incomplete filling of the radiometer beamwidth (i.e., beam filling errors) resulting from direct conversion of observed brightness temperatures to rainfall through radiative transfer model.

2. Development of the relationship between such bias errors and the antenna resolution as a function of brightness temperature parameters.

3. Development of a method based on this relationship and estimates of the brightness temperature parameters derivable from the observations for unbiased estimates of the mean rainfall.

4. Assessment of the quality of this method in terms of expected accuracy and confidence levels.

5. Computer simulation to validate that the bias correction method developed performs as expected.

The GATE* radar observations during the summer of 1974 proved to be nearly ideal for this study. They were used to derive the statistical properties typical of rainfall that were essential to this study and they were also used in the computer simulations after converting the radar measurements of rainfall into corresponding brightness temperatures using the radiation transfer model of Wilheit, et. al. [1977]. The details concerning construction of the brightness temerature scenes are presented in Section 2. The beam-filling problem is presented in Section 3. The formulas and relationships necessary to attain the objectives of this study are presented in Section 4. A discussion of the simulation results is presented in Section 5 and a summary is given in Section 6.

* GATE (Global Atmospheric Research Program) Atlantic Tropical Experiment.

2.0 RADIATION TRANSFER MODEL AND PREPARATION OF THE SIMULATED DATA

This section briefly describes the radiation transfer model of Wilheit, et. al. [1977] as it applies to the estimation of rainfall from brightness temperature observations and to our conversion of the GATE radar data into simulated brightness temperature scenes.

2.1 Rainfall Rate and Brightness Temperature Relationship

The thermal microwave radiation from the ocean surface as seen from space is modified by the liquid water and water vapor within the intervening atmosphere. The emissivity of the surface depends on its dielectric constant which for ocean surfaces varies approximately inversely with water temperature (T_W). However, at an incidence angle of approximately 55^o and in the region of 19 Ghz, these are nearly compensating factors. As a result, the brightness temperature (T_B) which is the product of emissivity and water temperature is nearly constant for smooth water. The wind at the water surface can effect the emissivity, but this effect is relatively insignificant. Therefore, the ocean presents a nearly uniform background radiation source so that variation in the received radiation results from variations in the attenuation of the radiation that are mostly due to variations in the liquid water content of the atmosphere.

The equation of radiative transfer through the atmosphere given by Wilheit, et. al. [1977] is

$$\frac{dT_B(\theta)}{dZ} + \alpha T_B(\theta) = S \int_0^{\pi} T_B(\theta_S) F(\theta, \theta_S) \text{ Sin } \theta_S \, d\theta_S + aT_Z \quad (2.1)$$

where;

$T_B(\theta)$ = radiance (or brightness temperature) in the direction specified by the polar angle θ,

α = total attenuation coefficient,

S = scattering coefficient,

a = absorption coefficient ($\alpha = a + S$),

T_Z = thermodynamic temperature of the atmosphere; and

$F(\theta, \theta_S)$ = scattering distribution function for scattering from angle θ_S to θ.

In 2.1, the absorption is attributed to all causes including gases, water droplets, water vapor, and ice crystals. At wavelength near 1 to 2 cm, only molecular oxygen, water vapor and water droplets are taken into account. However, contributions to the total absorbtion due to molecular oxygen and water vapor are relatively small and assumed values are used. The contribution of water droplets was calculated using Mie theory and a raindrop size distribution given by the Marshall-Palmer distribution,

$$N(r) = N_0 \, e^{-\delta r} \tag{2.2}$$

where, $N(r)$ is the number density of droplets per unit size interval, r is the radius of the droplets in centimeters, N_0 is 0.16 cm^{-4}, and

$$\delta = 81.56 \, R^{-0.21}. \tag{2.3}$$

In 2.3, R is the rain rate in mm hr^{-1}. Equations (2.2) and (2.3) provide the relationship between $N(r)$ and R, needed to solve equation (2.1) for T_B as a function of R.

The relationship between T_B and R was solved by Wilheit, et. al. [1977] for a layered atmosphere assumed to have water droplets from the freezing level to the surface. They modeled the water vapor content by the specifying a linear variation in humidity from the surface to the freezing level and they assumed that cloud water droplets have a density of 25 mg cm^{-2} for the first 0.5 km below the freezing level. Results of their calculations with an assumed lapse rate of 6.5°C per km are displayed in Figure 2-1 where the freezing level has been left as a free parameter. It should be pointed out that their model indicates that the brightness temperature increases monotonically with rain rate only up to 20 to 50 mm hr^{-1} after which the back-scatter of larger rain-drops causes a decrease in brightness temperature.

2.2 Simulation of Brightness Temperature Data

The radar measurements of rainfall, collected during the summer of 1974, over the GATE B-scale area, located approximately 1000 km off the west coast of Africa, are described in detail by Hudlow [1979]. The radar data used was specifically prepared for this study by the NOAA (National Oceanic and Atmospheric Administration) which provided the processed digital data (for Phases I and II) for each 4km x 4km rain cell at the original 15 minute observation intervals. A description of this specifically prepared GATE radar data is given by Laughlin and Gupta [1980]. It is recognized that although the radar measurements of rainfall may be somewhat erroneous, this will not have any significant effects in this study as long as the simulated ESMR has resolution larger than 4 km and has sampling interval larger than 15 minutes.

ORIGINAL PAGE IS
OF POOR QUALITY

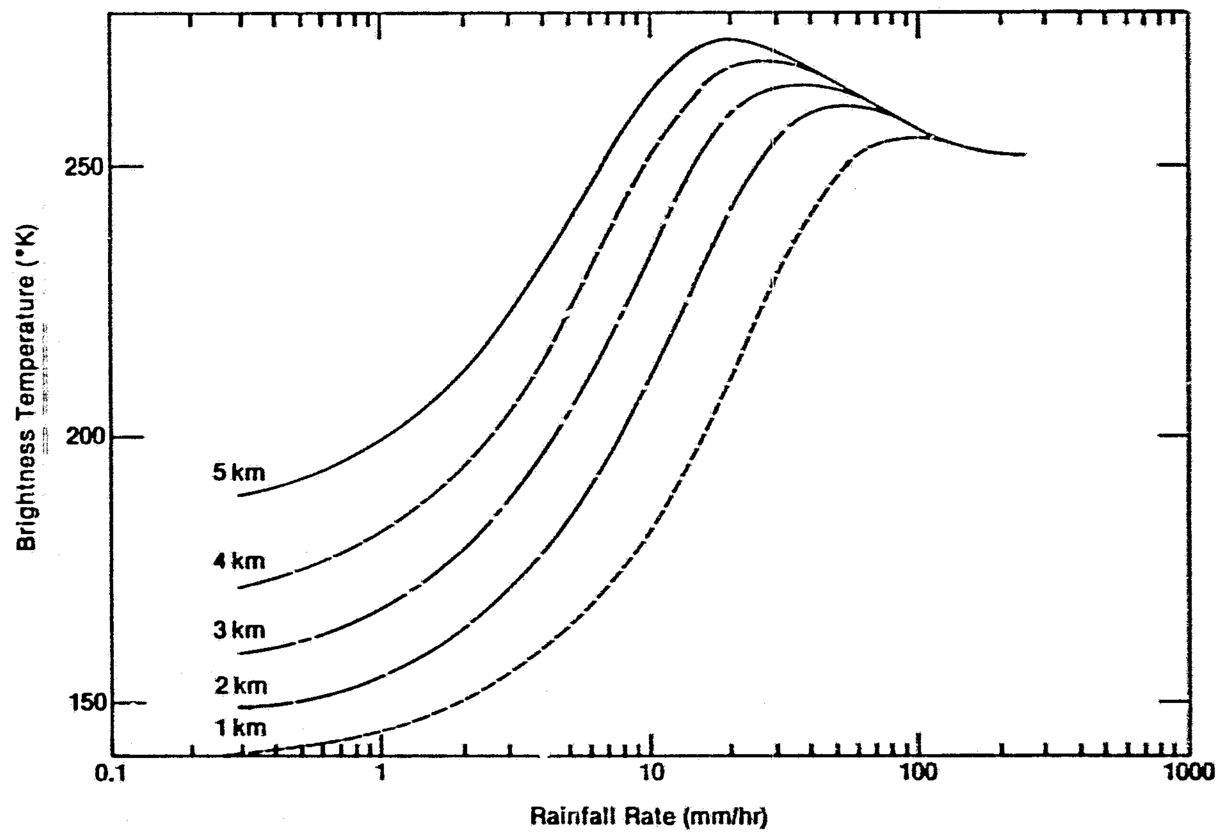

Figure 2-1
Calculated Brightness Temperatures at 1:55 CM as a Function of Rain Rate for Melting Levels of 1, 2, 3, 4, and 5 KM (from Wilheit, et al., 1977)

Each precipitation field consisting of an array of 100x100 cells was mapped into a corresponding brightness temperature field using the transformation curve of Figure 2-1. This transformation was done for each individual 4km x 4km cell in the precipitation (rain) field. A freezing level of 4km was assumed without any loss of generality. For computational ease, the best analytical fit for this transformation curve was found and has the following form,

$$T_B = 271 - 107\exp(-0.182\,R) \quad \text{for } R \leq 20 \text{ mm/hr} \qquad (2.4)$$
$$= 271 - 0.1944\,(R-20) \quad \text{for } R > 20 \text{ mm/hr}$$

This is a nonlinear relationship between R and T_B and, as will be seen later, introduces some error while estimating mean rainfall from observed brightness temperatures. These simulated brightness temperature fields formed the basis and provided the data for all the analysis performed in this study.

3.0 ERROR IN ESTIMATING RAINFALL FROM BRIGHTNESS TEMPERATURE

The accuracy with which passive radiometers can estimate rainfall from observed or simulated brightness temperatures depends on several factors. These include the non-linear and non-singular behavior of the T_B vs. R relationship, temporal sampling rate, and the spatial resolution of the antenna. The behavior of T_B and R relationship reflects the instrumental errors such as biasing of rainfall measurements due to incomplete filling of the radiometer beamwidth. These problems are addressed in this section.

3.1 Beam Filling Problem

Non-uniform and incomplete filling of the radiometer beam-width in conjunction with the fact that T_B vs. R relationship is non-linear and non-singular introduces a bias in the estimate of mean rainfall and this bias causes the rainfall to be consistently underestimated.

To understand this problem, let us examine a field-of-view (fov) of sufficiently large area such as 64km x 64km formed from an array of n cells with the cell size being much smaller in area than that of the fov. Assuming that the radiometer antenna has a resolution equal to cell size, the radiometer will measure the average brightness temperature, T_{bi} , in cell i for each cell in the fov.

The mean rainfall, $\bar{R}_1$, over the fov is then obtained according to equation (3.1).

$$\bar{R}_1 = \frac{1}{n} \sum_{i=1}^{n} f^{-1} (T_{bi}) \tag{3.1}$$

Where, f^{-1} represents the inverse transformation for converting brightness temperatures (T_{bi}) into corresponding rain rates (r_i). This is easily obtained from equation (2.4) and expressed as:

$$f^{-1} \; r_i = \frac{1}{c} \ln \left(\frac{b}{a - T_{bi}} \right) \tag{3.2}$$

where, a=271.0, b=107.0, and c=0.182 are constants.

In order to determine the existence of bias in estimating rainfall from observed brightness temperatures, let us now scan the same fov with another radiometer having an antenna of lower resolution such as k times the cell size, k being a positive integer greater than 1. The mean rainfall, $\bar{R}_2$, over the same fov can be obtained according to equation (3.3).

$$\bar{R}_2 = \frac{k}{n} \sum_{j=1}^{n/k} f^{-1} \left(\frac{1}{k} \sum_{\ell=(j-1)k+1}^{jk} T_{b\ell} \right) \tag{3.3}$$

The existence of bias will be positively confirmed if the quantity $\bar{R}_1 - \bar{R}_2$ is positive. In addition, the value of this quantity would indeed be the amount of bias error. To obtain a simple expression for $\bar{R}_1 - \bar{R}_2$, let us substitute equation (3.2) in equations (3.1) and (3.3) and simplify.

$$\bar{R}_1 - \bar{R}_2 = \frac{1}{nc} \sum_{i=1}^{n} \ln \left(\frac{b}{a - T_{bi}} \right) - \frac{k}{nc} \sum_{j=1}^{n/k} \ln \left(\frac{b}{a - \frac{1}{k} \sum_{\ell=(j-1)k+1}^{jk} T_{b\ell}} \right)$$

$$= -\frac{1}{nc} \sum_{i} \ln \left(1 - \frac{T_{bi}}{a} \right) + \frac{k}{nc} \sum_{j} \ln \left(1 - \frac{\frac{1}{k} \sum_{\ell} T_{b\ell}}{a} \right)$$

ORIGINAL PAGE IS
OF POOR QUALITY

Using a series expansion: $\ell n(1+x) = x - \frac{x^2}{2} + \frac{x^3}{3} - \frac{x^4}{4} + \ldots\ldots\ldots,$
and simplifying:

$$\bar{R}_1 - \bar{R}_2 = \frac{1}{nc} \sum_i \left[\frac{T_{bi}}{a} + \frac{1}{2}\left(\frac{T_{bi}}{a}\right)^2 + \frac{1}{3}\left(\frac{T_{bi}}{a}\right)^3 + \ldots\ldots\ldots, \right]$$

$$- \frac{k}{nc} \sum_j \left[\frac{\frac{1}{k} \sum_\ell T_{b\ell}}{a} + \frac{1}{2}\left(\frac{\frac{1}{k} \sum_\ell T_{b\ell}}{a}\right)^2 + \frac{1}{3}\left(\frac{\frac{1}{k} \sum_\ell T_{b\ell}}{a}\right)^3 + \ldots\ldots\ldots \right]$$

$$= \frac{1}{c} \left[\frac{m_{2,1} - m_{2,k}}{2a^2} + \frac{m_{3,1} - m_{3,k}}{3a^3} + \frac{m_{4,1} - m_{4,k}}{4a^4} + \ldots\ldots\ldots \right]$$

$$= \frac{1}{c} \sum_{p=2}^{\infty} \left(\frac{m_{p,1} - m_{p,k}}{p\ a^p} \right) \qquad (3.4)$$

Where, $m_{p,1}$ represents the p^{th} empirical moment of brightness temperatures observed with antenna having a resolution equal to cell size and $m_{p,k}$ represents the p^{th} empirical moment of brightness temperatures observed with antenna having a resolution equal to k times the cell size. A close examination of equation (3.4) reveals that each term in the summation is positive and that the entire series is convergent. Furthermore, it is clear tha as k increases each term in the summation also increases. As a result, the following conclusions can be made.

1. There is a bias error in estimating rainfall from brightness temperature.

2. This bias error is computable and is given by equation (3.4). The accuracy of computation depends on the place of truncation.

3. The bias error increases as the antenna resolution decreases.

Various methods for removing this bias are possible. The technique presented in the next section deals with estimating population variance i.e., (limiting value of variance as antenna resolution becomes higher and higher) from observed (or simulated) brightness temperatures. This technique has worked exceedingly well.

3.2 Error Due to Non-Uniqueness of T_B and R Relationship

It is clear from Figure 2-1 that T_B and R relationship is not unique when estimating rainrate for observed brightness temperature, i.e., an observed T_B will result in two different values of R according to equation (2.4). Similarly, during simulation of ESMR data from GATE radar data two different rain rates may result in a single value for brightness temperature. For example, R=10 and R=109.5 mm/hr both map into $T_B = 253.6^{\circ}K$. Thus the simulated ESMR data inherently contains an error component which cannot be removed easily. Experimental results to indicate the magnitude of this error are presented in Section 5.

4.0 UNBIASED ESTIMATION TECHNIQUE FOR MEAN RAINFALL

This section deals with a mathematical formulation for the problem of finding an unbiased estimator of true mean rainfall based upon the brightness temperature measurements made by ESMR like instruments, the physical characteristics of ESMR involved in the derivation of T_B and R relationship, and adequate knowledge of the rainfall rate distribution. Also presented in this section are an estimation technique and a methodology for a practical implementation.

4.1 Frequency Distribution of Rainfall Rate

The frequency distribution analysis of GATE radar measured rainfall data was carried out for various fov's in the range 4km x 4km to 256km x 256km. For most fov's, this analysis indicated that rainfall rate, R, follows Gamma distribution. Figure 4-1 illustrates an example for the case when fov is 8km x 8km. The rain rate Gamma density function, $f_R(R, \alpha_R, \beta_R)$, can be expressed as in equation (4.1), where α_R and β_R are the two parameters.

$$f_R\left(R,\alpha_R,\beta_R\right) = \frac{\beta_R^{\alpha_R}}{\Gamma\alpha_R} \exp\left(-\beta_R R\right) R^{\left(\alpha_R-1\right)} \qquad (4.1)$$

It should be noted that both α_R and β_R are positive.

The frequency analysis also showed that the rainrate exceeded 20 mm/hr in less than 2 percent of the observations. As a result, for the sake of simplicity, one can truncate the T_B and R functional relationship of equation (2.4) at R in excess of 20 mm/hr so that equation (2.4) can be rewritten as:

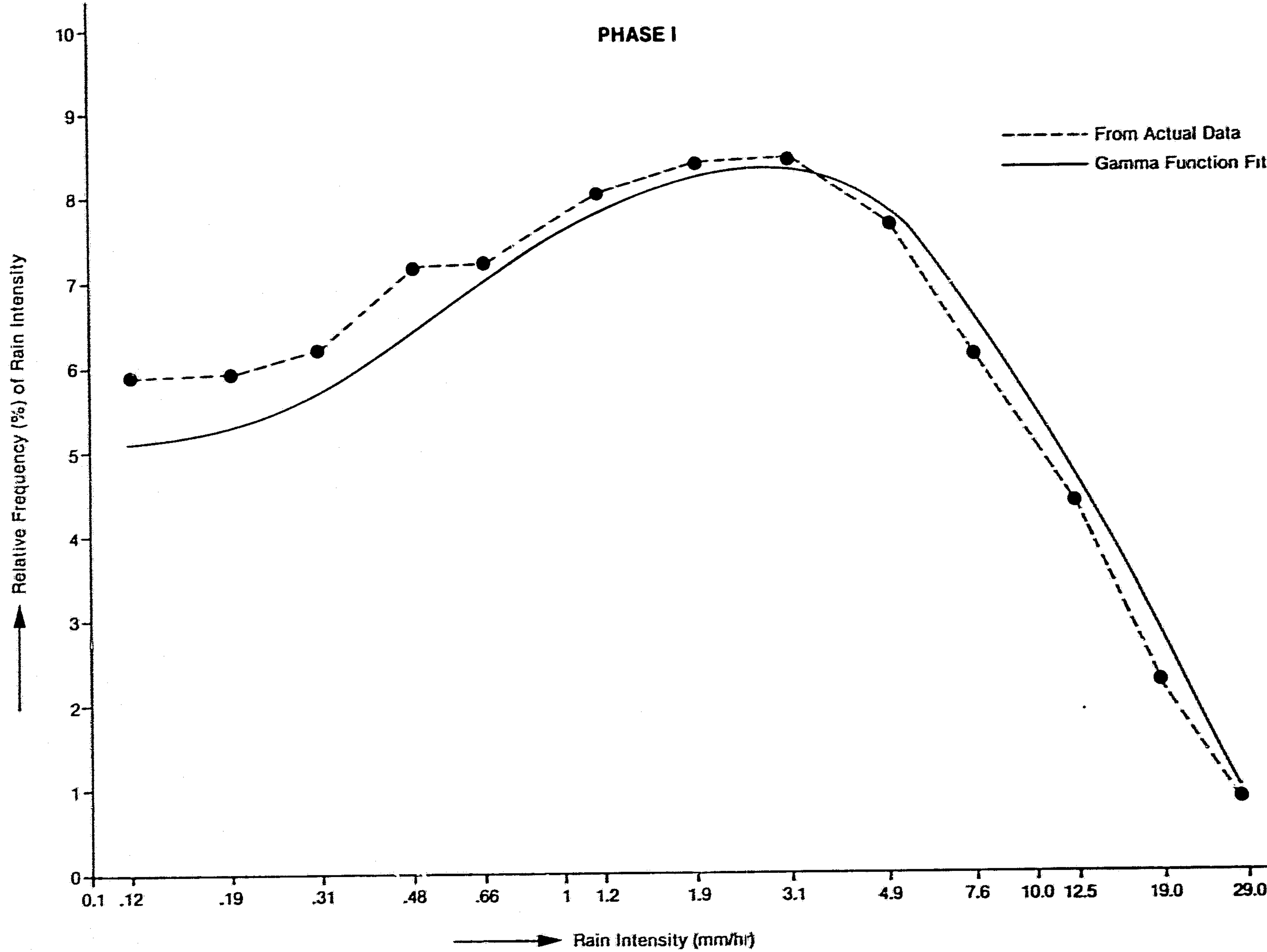

Figure 4-1
Rain Intensity Distribution for 8 KM Resolution

$$T_B = F(R) = a - b \exp(-cR) \qquad (4.2)$$

Where, a=271, b=107, and c=0.182 are constants. Knowing the general form of rain rate density function and the T_B and R functional relationship, one can find the density function of brightness temperatures, $f_T(T_B, \alpha_T, \beta_T)$, as follows (see Papoulis [1965]);

$$f_T(T_B, \alpha_T, \beta_T) = \frac{f_R(R, \alpha_R, \beta_R)}{F'(R)} \qquad (4.3)$$

Where F'(R) is the first derivative of F(R) in equation (4.2). It should be noted that $f_T(T_B, \alpha_T, \beta_T)$ is also a Gamma density function with parameters α_T and β_T, both parameters being positive. Furthermore, from properties of Gamma distribution, the mean brightness temperature M_T (or $\bar{T}$) and the variance $\sigma_T{}^2$ can be expressed in terms of α_T and β_T as given below.

$$\alpha_T = \frac{\bar{T}^2}{\sigma_T{}^2}$$

and,

$$\beta_T = \frac{\bar{T}}{\sigma_T{}^2} \qquad (4.4)$$

Similarly,

$$\alpha_R = \frac{\bar{R}^2}{\sigma_R{}^2}$$

and

$$\beta_R = \frac{\bar{R}}{\sigma_R{}^2} \qquad (4.5)$$

where, M_R (or $\bar{R}$) is the mean rainfall and $\sigma_R{}^2$ is the variance.

The problem of estimating true mean rainfall can now be stated as follows: given an estimate of $\bar{T}$ and $\sigma_T{}^2$ as obtained from simulated ESMR data; the functional relationship between brightness temperature and rain rate; and the form of rain rate distribution, find an estimate of mean rainfall, $\hat{R}$ (or $\hat{M}_R$). The mathematical details of this estimation technique are presented below.

4.2 Mean Rainfall Estimation Technique

The essence of the technique to be presented here is to estimate $\hat{R}$ from the observed mean brightness temperature, $\bar{T}$, and the variance, σ_T^2, of brightness temperature within a field of view. However, in order to facilitate easier understanding, α_R and β_R, the parameters of rainfall rate distribution would be estimated first. An estimate of mean rainfall can then be easily obtained from equations (4.5).

The mean brightness temperature, $\bar{T}$, can be expressed as

$$\bar{T} = \int_0^\infty T_B \; f_T \; (T_B, \alpha_T; \beta_T) \; dT$$

Substituting for $f_T(T_B , \alpha_T , \beta_T)$ from equation (4.3) and using the fact that $dT = F'(R)dR$, $\bar{T}$ becomes

$$\begin{aligned} \bar{T} &= \int_0^\infty F(R) \; \frac{f_R \; (R, \alpha_R, \beta_R)}{F'(R)} \; F'(R) \; dR \\ &= \int_0^{20} (F(R) \; f_R(R, \alpha_R, \beta_R) \; dR \end{aligned} \qquad (4.6)$$

Using the expression for F(R) from equation (4.2) and the expression for $f_R(R, \alpha_R , \beta_R)$ from equation (4.3) and simplifying, equation (4.6) results in the following.

$$\bar{T} = a - b \frac{(\beta_R)^{\alpha_R}}{(\beta_R+c)^{\alpha_R}} \tag{4.7}$$

The intermediate steps used in deriving equation (4.7) are presented in Appendix A.

The next step in the present estimation technique is to express σ_T^2 in terms of α_R and β_R. The variance, σ_T^2, can be expressed as $E[T_B^2] - \bar{T}^2$, where $E[T_B^2]$ is the mean squared brightness temperature and can be expressed as in equation (4.8).

$$E\,[T_B^2] = \int_0^\infty T_B^2 \; f_T(T_B, \alpha_T, \beta_T) \; dT \tag{4.8}$$

Once again, using the substitutions and simplifying in a manner similar to the ones used in deriving equation (4.7), we obtain:

$$E\,[T_B^2] = a^2 - 2ab \left(\frac{\beta_R}{\beta_R+c}\right)^{\alpha_R} + b^2 \left(\frac{\beta_R}{\beta_R+2c}\right)^{\alpha_R} \tag{4.9}$$

The variance, σ_T^2, can now be expressed as follows:

$$\begin{aligned} \sigma_T^2 &= E\,[T_B^2] - \bar{T}^2 \\ &= b^2 \left[\left(\frac{\beta_R}{\beta_R+2c}\right)^{\alpha_R} - \left(\frac{\beta_R}{\beta_R+c}\right)^{2\alpha_R} \right] \end{aligned} \tag{4.10}$$

Appendix A contains necessary steps used in deriving equations (4.9) and (4.10).

Equations (4.7) and (4.10) express $\bar{T}$ and σ_T^2, respectively, in terms of parameters α_R and β_R. Further simplifications, presented in detail in Appendix A, result in the following;

ORIGINAL PAGE IS
OF POOR QUALITY

$$\alpha_R = \frac{L_1}{\left[\ln\beta_R - \ln\left(\beta_R+c\right)\right]} \tag{4.11}$$

and,

$$\left(\beta_R+c\right)^{L_2+2L_1} - \beta_R^{\,L_2+L_1}\left(\beta_R+2c\right)^{L_1} = 0 \tag{4.12}$$

Where, L_1 and L_2 are functions of known quantities and are expressed as:

$$L_1 = \ln\left(\frac{a - \bar{T}}{b}\right) \tag{4.13}$$

and,

$$L_2 = \ln\left[\frac{\sigma_T^{\,2}}{\left(a - \bar{T}^2\right)} + 1\right] \tag{4.14}$$

Note that $\bar{T}$ and σ_T^2 are known since they can be computed from simulated ESMR data and a, b and c are constants used in equation (4.2) earlier.

Equations (4.11) and (4.12) express α_R and β_R in terms of known quantities. However, unfortunately, these equations cannot be solved to give estimates of α_R and β_R in closed forms. As a result, one must use numerical methods to solve for α_R and β_R from these equations. An estimate of mean rainfall is then obtained from equations (4.5).

It should be emphasized that the estimation technique presented in this subsection is valid for all fov's as long as the area of fov under consideration is at least equal to the spatial resolution of the antenna on the radiometer.

4.3 Analysis to Determine Spatial Correlation

Spatial correlation is an important parameter because it provides a measure of the characteristic rain cell size and, as a result, its determination will prove useful in the choice of adequate resolution for passive microwave radiometers.

One way to formulate the problem is to consider the simulated ESMR data as a time series x(t), where x(t) represents a brightness temperature scene at time instant t. Each scene in this time series can be considered either as a spatial array of equal size cells or as a much longer linear array formed by taking consecutive rows or columns (from the spatial array) and placing them in a single row or column. For easier understanding of the mathematical details to follow, a linear array representation is used. To remove the time variability, the time series x(t) is time-averaged to result in a single or master scene X. Note that this scene X may have high spatial variability.

To study the spatial variability, the master scene, X, is scanned with different size antennas. Let D_a represent the averaging distance of antenna under consideration. ESMR like radiometers, being integrating instruments, will provide individual brightness temperatures, $T_B(D_a)$, which are distance D_a apart from each other and can be expressed as in equation (4.15).

$$T_B(D_a) = \frac{1}{D_a} \int_0^{D_a} X(D) \quad dD \qquad (4.15)$$

Equation (4.15) emphasizes spatial variability by using X(D) to represent the master scene X, where D denotes distance.

It is clear that the mean brightness temperature, T_B, of master scene is independent of D_a since it represents the average of averages. However, the variance, $\sigma_T^2(D_a)$, is a more useful statistical parameter and is definitely dependent on D_a. It can be expressed as

$$\sigma_T^2\,(D_a) = E\left[\left\{T_B(D_a) - \bar{T}_B\right\}\left\{T_B(D_a) - \bar{T}_B\right\}\right] \tag{4.16}$$

Using equation (4.15) and simplifying, one obtains

$$\sigma_T^2\,(D_a) = E\left[\frac{1}{D_a^2}\left\{\int_0^{D_a} X(D_1)\,dD_1 - \bar{T}_B\right\}\left\{\int_0^{D_a} X(D_2)\,dD_2 - \bar{T}_B\right\}\right]$$

$$= \frac{1}{D_a^2}\int_0^{D_a}\int_0^{D_a} R_X(D_1 - D_2)\,dD_1\,dD_2$$

$$= \frac{2}{D_a}\int_0^{D_a}\left(1 - \frac{D'}{D_a}\right) R_X\left(D'\right)\,dD' \tag{4.17}$$

(see Davenport and Root, p 69)

Where $R_x(D')$ is spatial autocovariance function and is assumed to be exponential. Equation (4.17) can be further simplified to express $\sigma_T^2(D_a)$ as in equation (4.18). A detailed derivation of equation (4.18) is presented in Appendix B.

$$\sigma_T^2(D_a) = 2\sigma_X^2\left[\frac{1}{y} + \frac{1}{y^2}\left(-1 + \exp\,(-y)\right)\right] \tag{4.18}$$

Where, σ_x^2 is the population variance or, alternatively, the maximum value of $R_x(D)$. And $y = \frac{D_a}{D_o}$, D_o being the correlation distance.

The term correlation distance can be defined in a number of ways. For example, it can be defined as that value of averaging distance, D_a, for which $R_x(D)$ equals approximately 37 percent of its maximum value, $R_x(o)$. Alternatively, D_o may be defined as that value of D_a for which σ_T^2 equals approximately 73 percent of σ_x^2.

The population variance and the correlation distance can both be estimated according to equation (4.18) on the basis of as few as two calculated values of $\sigma_T^2(D_a)$ computed for two different values of D_a. An unbiased estimate of true mean rainfall can then be obtained from σ_x^2 and $\bar{T}_B$ by using the parameter estimation technique of subsection 4.2. This is discussed in more detail in the next subsection.

4.4 Removal of Bias Due to Non-Linearity

The estimation technique presented in subsection 4.2 works exceedingly well for all fov's and results in better estimation of mean rainfall than the one obtained by using transformation curve alone. However, it must be extended further in order to remove the bias in the estimate due to non-linearity of T_B and R relationship.

As discussed in Section 3.0, the errors in the estimate of mean rainfall are caused by bias and are not random errors. As a result, statistical averaging over all fov's in the GATE size area is not very helpful. One approach to reduce or even eliminate this bias would be to use radiometers having higher resolution, i.e., capable of remotely sensing the brightness temperatures over smaller and smaller areas. As a matter of fact, an ideal radiometer would be the one having the capability to measure brightness temperature at each point within the fov. However, improvements in radiometer resolution are limited by economical, engineering, and practical considerations since improvement in resolution translates into larger and larger antenna.

A practical approach to removing the bias is as follows: using the radiometer of given resolution, find from observed data the mean brightness temperature, $\bar{T}$, and the variance, σ_T^2, over several larger fov's; plot σ_T^2 versus the square root of the area of fov's ($\sqrt{A}$) and fit a multinomial function to obtain an analytical relationship between σ_T^2 and $\sqrt{A}$; and extrapolate this curve to obtain an estimate of population variance (σ_x^2), i.e., the value of σ_T^2 when $\sqrt{A}$ approaches zero. The estimated population variance and $\bar{T}$ will then be used to estimate mean rainfall by the technique described in subsection 4.2. The resulting estimate $\hat{R}$ will be unbiased since its expected value will be equal to the true mean rainfall. A detailed methodology for implementing this approach will be presented later in this section.

An alternate approach based upon the analysis of spatial correlation in subsection 4.3 has demonstrated good potential. In this approach, one needs to compute the variance, $\sigma_T^2(D_a)$, for only two different averaging distances. Based upon these computations, equation (4.18) is solved numerically, as described in

Appendix C, to give an estimate of population variance, σ_x^2, and an estimate of correlation distance, D_o. The next step is to find an unbiased estimate of true mean rainfall. This is done by the same technique as in the previous approach. Some preliminary results obtained using alternate approach are quite encouraging and will be discussed in Section 5.

4.5 Error Bounds on Estimate of Population Variance

The estimate of population variance, σ_x^2, as obtained by the technique described above will in general contain some error. This error is attributable, in large part, to the fact that the brightness temperatures can only be observed at discrete time intervals and *not* continuously. In otherwords, the sampling error can be used to determine error bounds on the estimate of population variance.

A detailed analysis of sampling error has been performed by Laughlin and Gupta [1980] which resulted in the following expression for sampling error, σ_e^2.

$$\sigma_e^2 = \frac{2\sigma_x^2}{(T/\tau_o)}\left[-1 + \frac{t_o}{2\tau_o}\left(\frac{e^{t_o/\tau_o}+1}{e^{t_o/\tau_o}-1}\right) + \frac{\left(e^{-T/\tau_o}-1\right)}{\left(T/\tau_o\right)}\left\{1 - \frac{t_o}{\tau_o}\left(\frac{e^{t_o/\tau_o}+1}{e^{t_o/\tau_o}-1}\right) + \left(\frac{t_o}{\tau_o}\right)^2 \frac{e^{t_o/\tau_o}}{\left(e^{t_o/\tau_o}-1\right)^2}\right\}\right] \tag{4.19}$$

Where, t_o is the sampling period, τ_o is the temporal correlation interval, and T is the record length. The errors in estimating σ_T^2 within each fov follow a normal distribution and, therefore, will be used to find error bounds to any desired confidence level. For example, within two standard deviations ($2\sigma_e$) the confidence level will be at 95%. As will be seen in Section 5., these error bounds are used to find mean error in estimating mean rainfall as a function of antenna resolution.

4.6 Methodology

The methodology for obtaining an unbiased estimate of mean rainfall as described earlier can be implemented as follows:

(a) From the simulated (or observed) data, compute the mean brightness temperature, $\bar{T}$, and the variance, σ_T^2, of brightness temperatures for several area fov's. Let A denote the area of an fov under consideration. Then $\sqrt{A}$ may be referred to as areal dimension or averaging distance.

(b) Plot σ_T^2 versus $\sqrt{A}$ and fit a multinomial function to obtain a functional relationship between the two. Note that $\bar{T}$ is same for all fov's, since in each case the averaging is done over common area size.

(c) Extrapolate the curve obtained in step (b) and obtain an estimate of population variance, σ_x^2. This represents the limiting value of σ_T^2 as $\sqrt{A}$ becomes diminishingly small. This will also provide an estimate of spatial correlation.

(d) Use estimated population variance, σ_x^2 and $\bar{T}$ to estimate the mean rainfall, $\hat{\bar{R}}$, according to the estimation technique described in Section 4.2. $\hat{\bar{R}}$ is an unbiased estimate of true mean rainfall.

(e) Use equation (4.19) to compute error bounds for desired confidence level.

This methodology was implemented on the simulated ESMR data. The results obtained and a discussion of those results are presented in the next section.

5.0 EXPERIMENTAL RESULTS AND DISCUSSION

Earlier work of Laughlin and Gupta [1980] and other investigators has shown that, from a sampling point of view, samples taken every six hours are adequate. As a result, the simulated data from Phase I resulted in 72 brightness temperatures scenes and that from Phase II resulted in 64 brightness temperature scenes. From each time series, the mean brightness temperature, $\bar{T}$, and variance, σ_T^2, of brightness temperatures was computed for seven different size fov's: 4km x 4km, 8km x 8km, 16km x 16km, 32km x 32km, 64km x 64km, 128km x128km, and 256km x 256km. In each case the averaging was done over a common area of size 256km x 256km and, therefore, $\bar{T}$ remains same for all fov's. However, σ_T^2 does not and, in fact, as expected, it decreases as the area of fov increases. Computed values of $\bar{T}$ and σ_T^2 are tabluated in Table 5-1.

To determine the extent of errors due to non-linearity and non-uniqueness of T_B and R relationship, the mean rainfall rate for each Phase was computed using the T_B and R relationship of equation (2.4). The results are shown in Table 5-2. This non-parametric method was also used to find mean error in mean rainfall and the error variance which are shown in Figures 5-1 through 5-4 for both Phases I and II. It is clear that both the mean error and the error variance increase with the size of the fov. Note that mean error is approximately 10 percent even for the smallest size fov. This error is due only to non-uniqueness of T_B and R relationship and non-linearity of this relationship does not affect it since no averaging was done for this fov.

TABLE 5-1

MEAN BRIGHTNESS TEMPERATURE AND VARIANCES

FOR PHASE I AND PHASE II

FOR VARIOUS FIELD OF VIEWS

		Field Of View						
Phase		4km	8km	16km	32km	64km	128km	256km
I	Mean Brightness Temperature $\bar{T}$	168.6	168.6	168.6	168.6	168.6	168.6	168.6
	Variance σ_T^2	267	230	190	150	105	70	30
II	Mean Brightness Temperature $\bar{T}$	167.4	167.4	167.4	167.4	167.4	167.4	167.4
	Variance σ_T^2	198	165	126	91	55	30	16

TABLE 5-2

TRUE AND ESTIMATED MEAN RAINFALL

FOR PHASE I AND II

OBTAINED BY NON-PARAMETRIC METHOD

Phase	True Mean Rainfall	Estimated Mean Rainfall Field Of View						
		4km	8km	16km	32km	64km	128km	256km
I	.468	.443	.379	.339	.309	.286	.269	.251
II	.368	.332	.272	.239	.215	.200	.190	.183

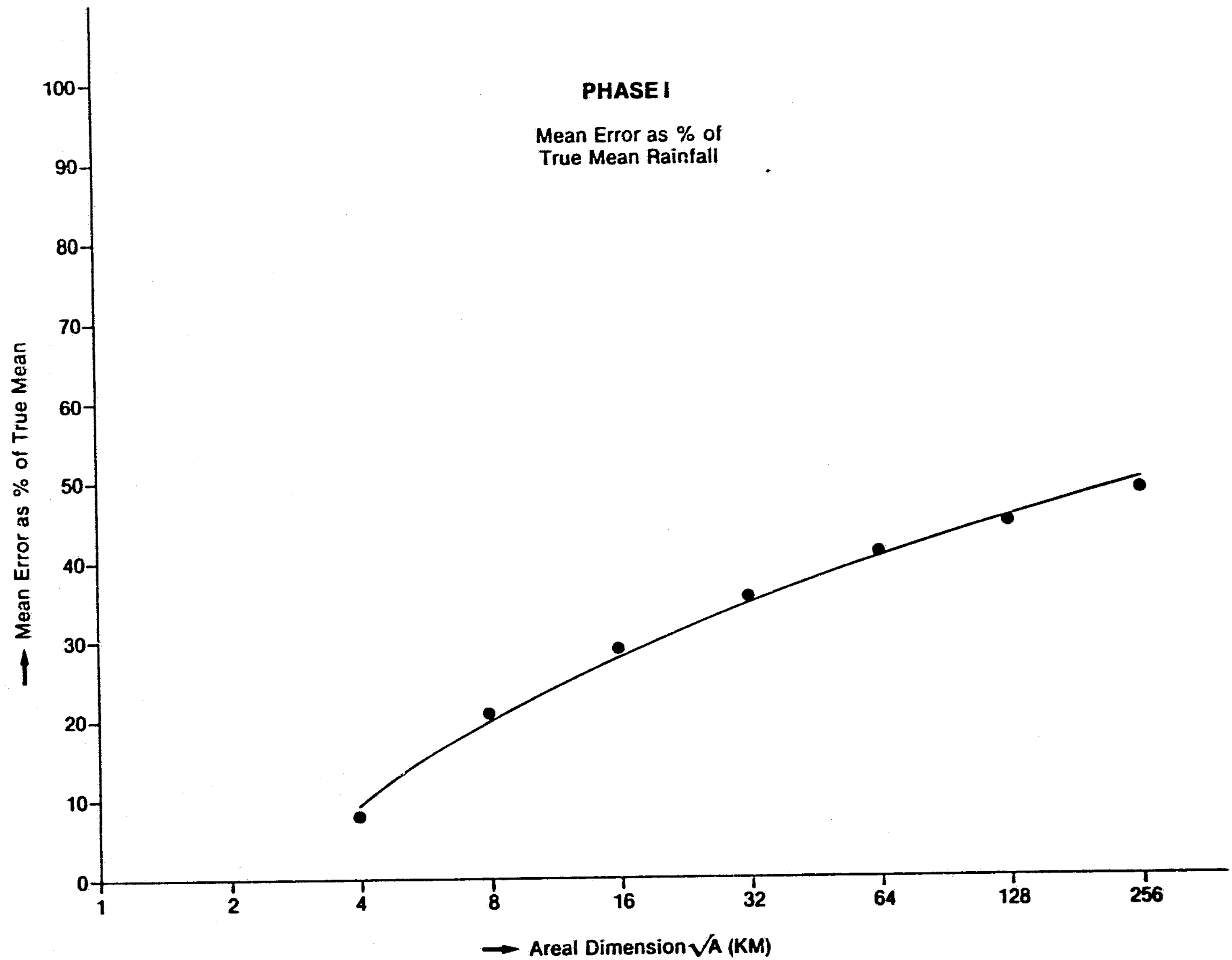

Figure 5-1
Mean Error as % of True Mean vs. Areal Dimension

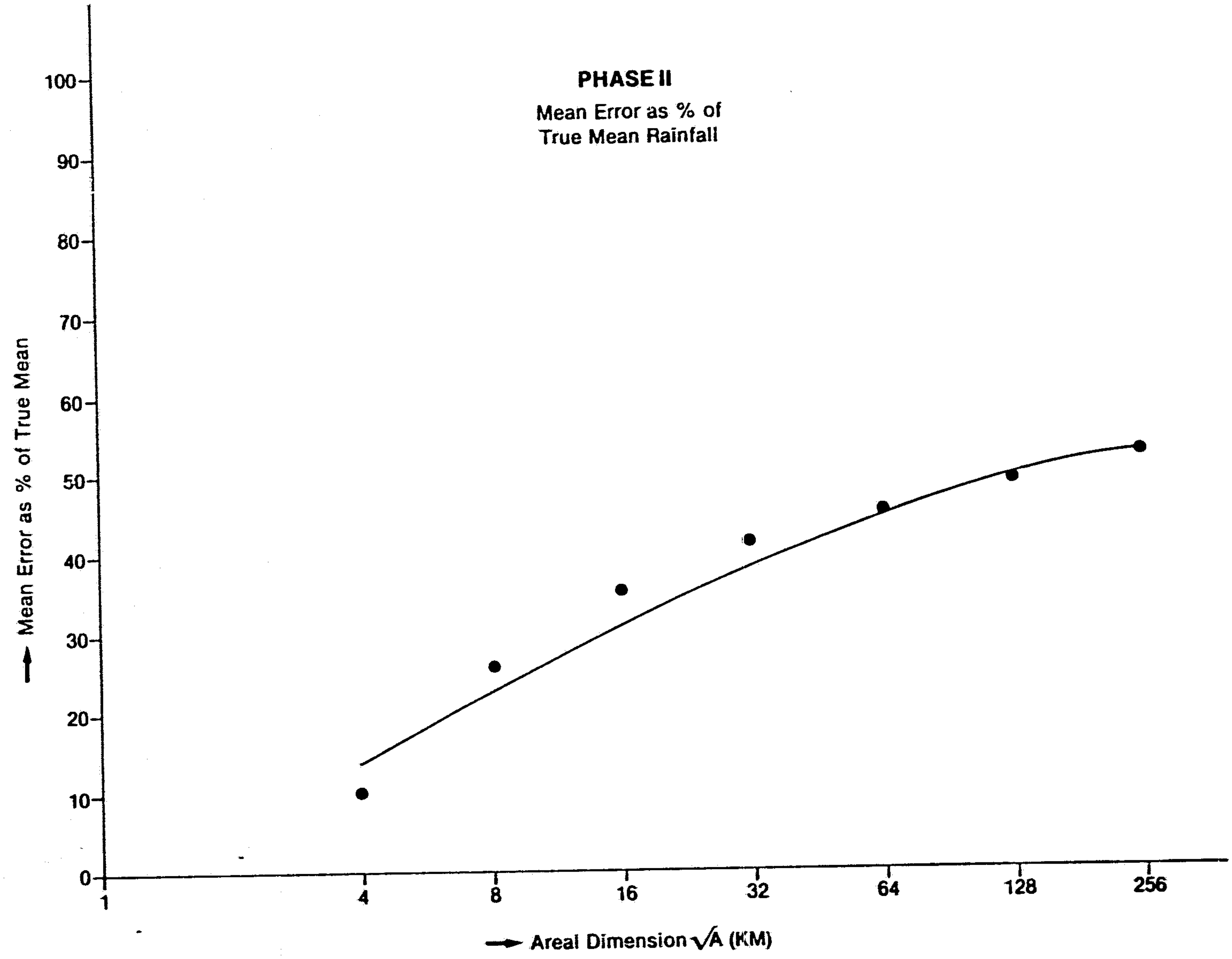

Figure 5-2
Mean Error as % of True Mean vs. Areal Dimension

ORIGINAL PAGE IS
OF POOR QUALITY

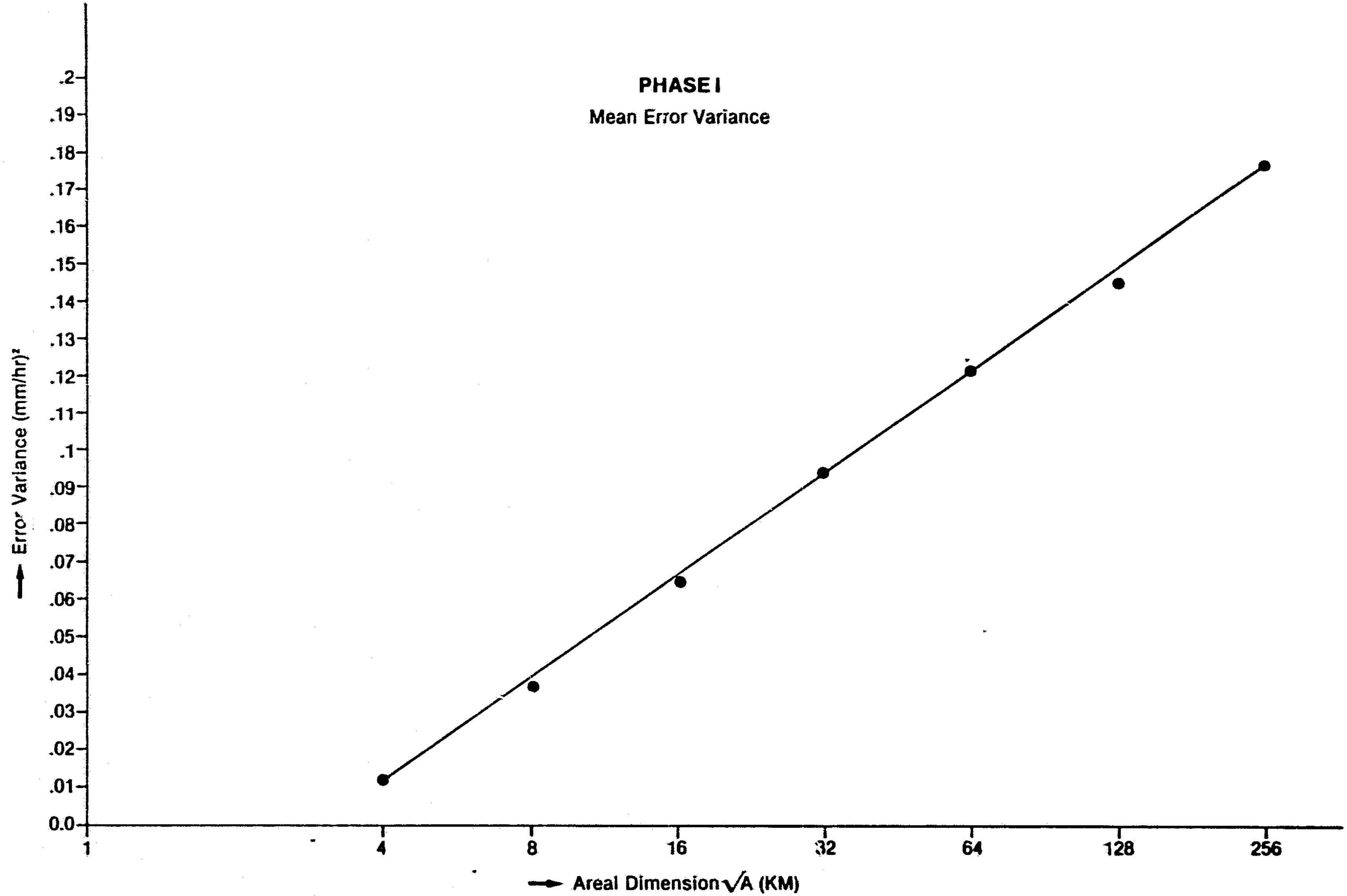

Figure 5-3
Error Variance vs. Areal Dimension

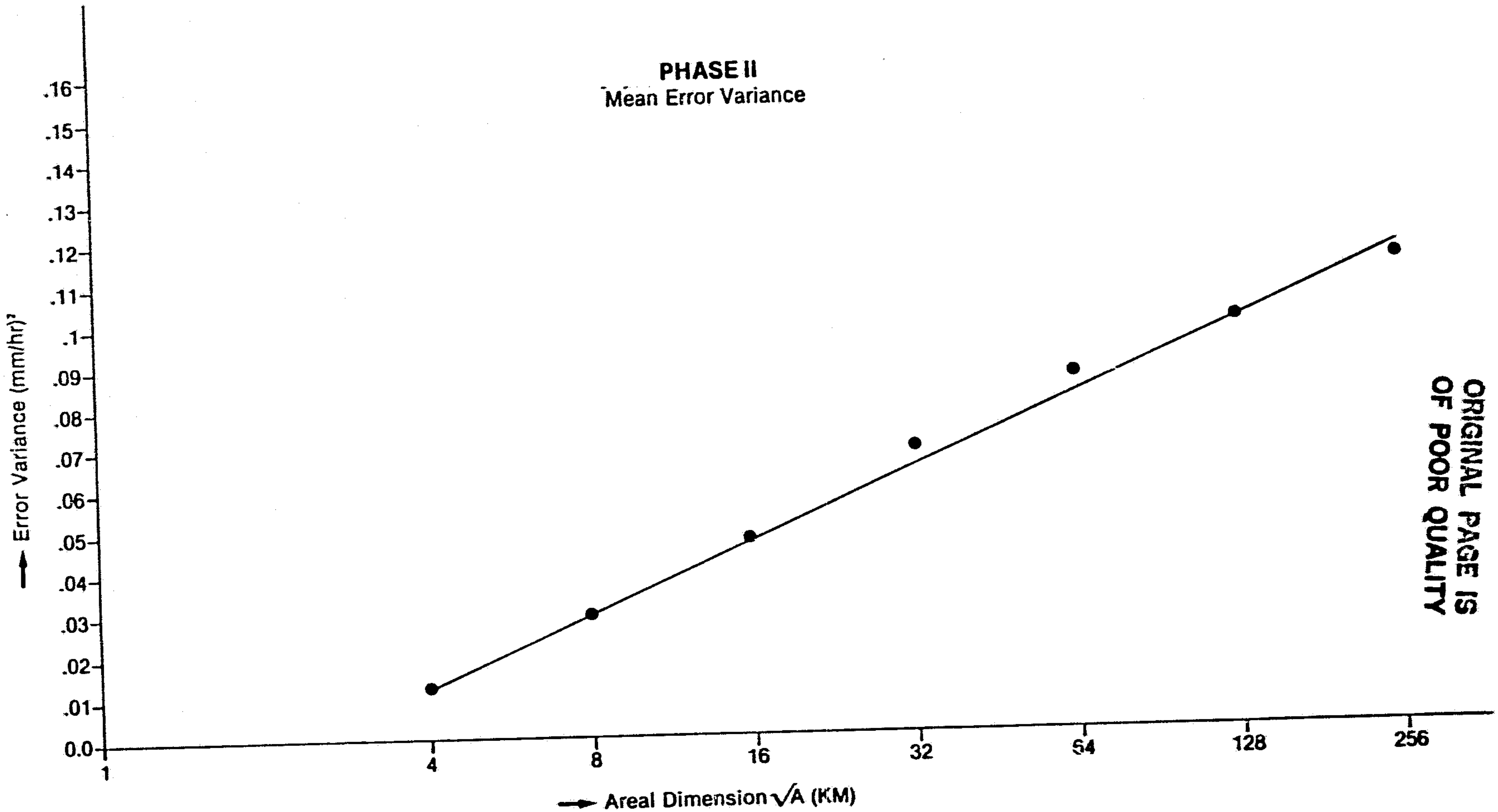

Figure 5-4
Error Variance vs. Areal Dimension

This error component can not be easily corrected since it is inherently present in the simulated data itself. It should be pointed out that the true mean rainfall rate (0.486 mm/hr^{-1} for Phase I and 0.368 mm/hr^{-1} for Phase II) as obtained from radar measurements was assumed to be correct for the above method. However, as will be seen later, even the radar measurements were underestimates.

The methodology described in subsection 4.6 was implemented using the values of $\bar{T}$ and σ_T^2 from Table 5-1. The polynomial fits of sixth order were obtained for σ_T^2 and were found to be very good approximations to the form in equation (4.18) which is expressed slightly differently in equation (5.1).

$$\sigma_T^2 = 2\sigma_x^2 \left[\sqrt{\frac{A_o}{A}} + \frac{A_o}{A} \left(-1 + e^{-\sqrt{A/A_o}} \right) \right] \quad (5.1)$$

where, $\sqrt{\frac{A}{A_o}}$ has the same interpretation as $\frac{D_a}{D_o}$ in Section 4. The results are shown in Figures 5-5 and 5-6 for Phases I and II, respectively. The population variance, σ_x^2, is estimated to be 310 for Phase I and 230 for Phase II. The spatial correlation, $\sqrt{A_o}$, is estimated to be 10km for Phase I and 8km for Phase II. The parameter estimation technique of subsection 4.2 resulted in the unbiased estimate of mean rainfall rate, $\hat{R}$. These results are tabulated in Table 5-3. The unbiased estimates are approximately 35 percent above the radar measurements which were made over 4km x 4km rain cells. This clearly demonstrates that even at 4km there exists a significant beam filling problem. At the

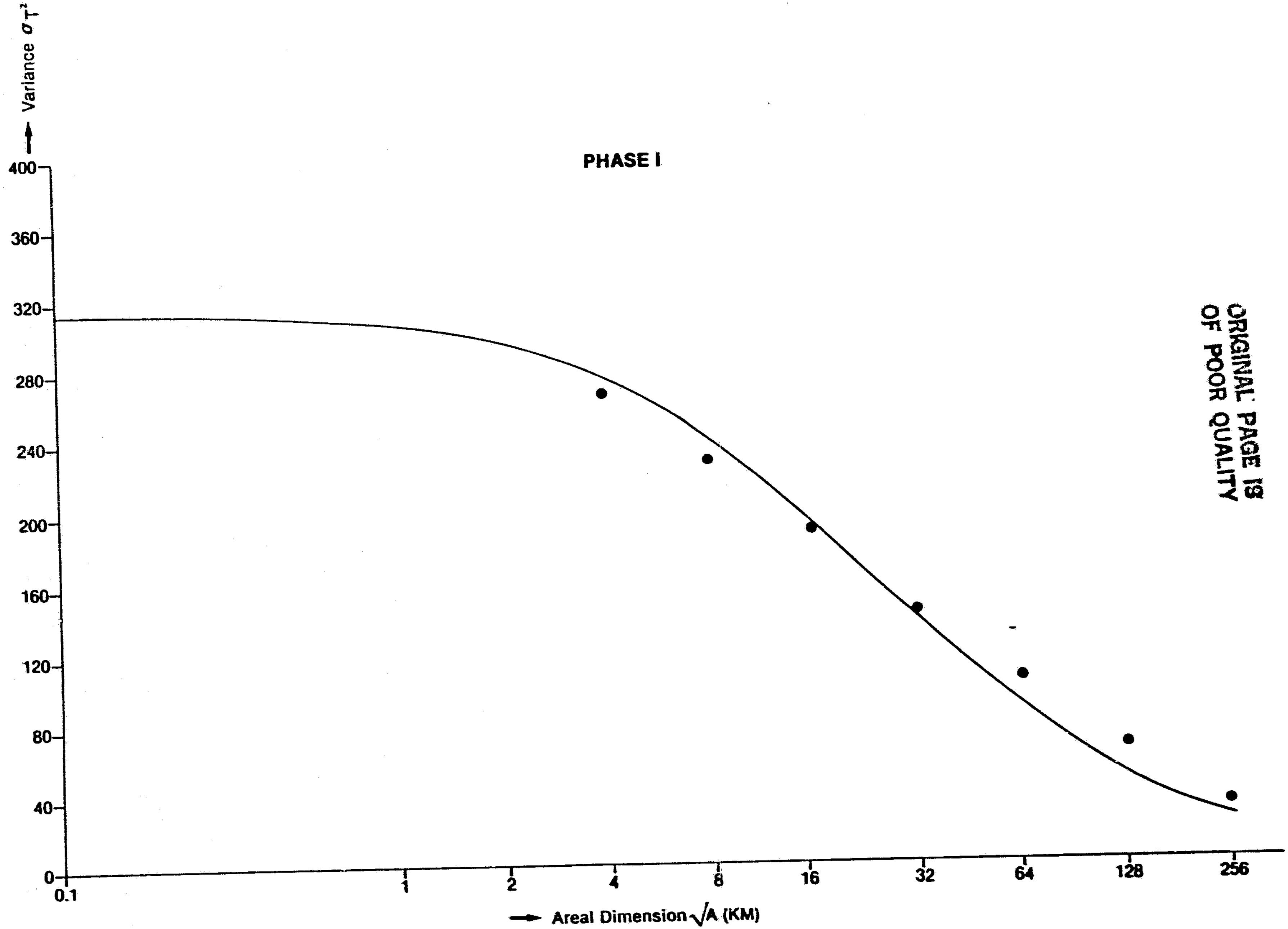

Figure 5-5

Variance σ_T^2 vs. Areal Dimension

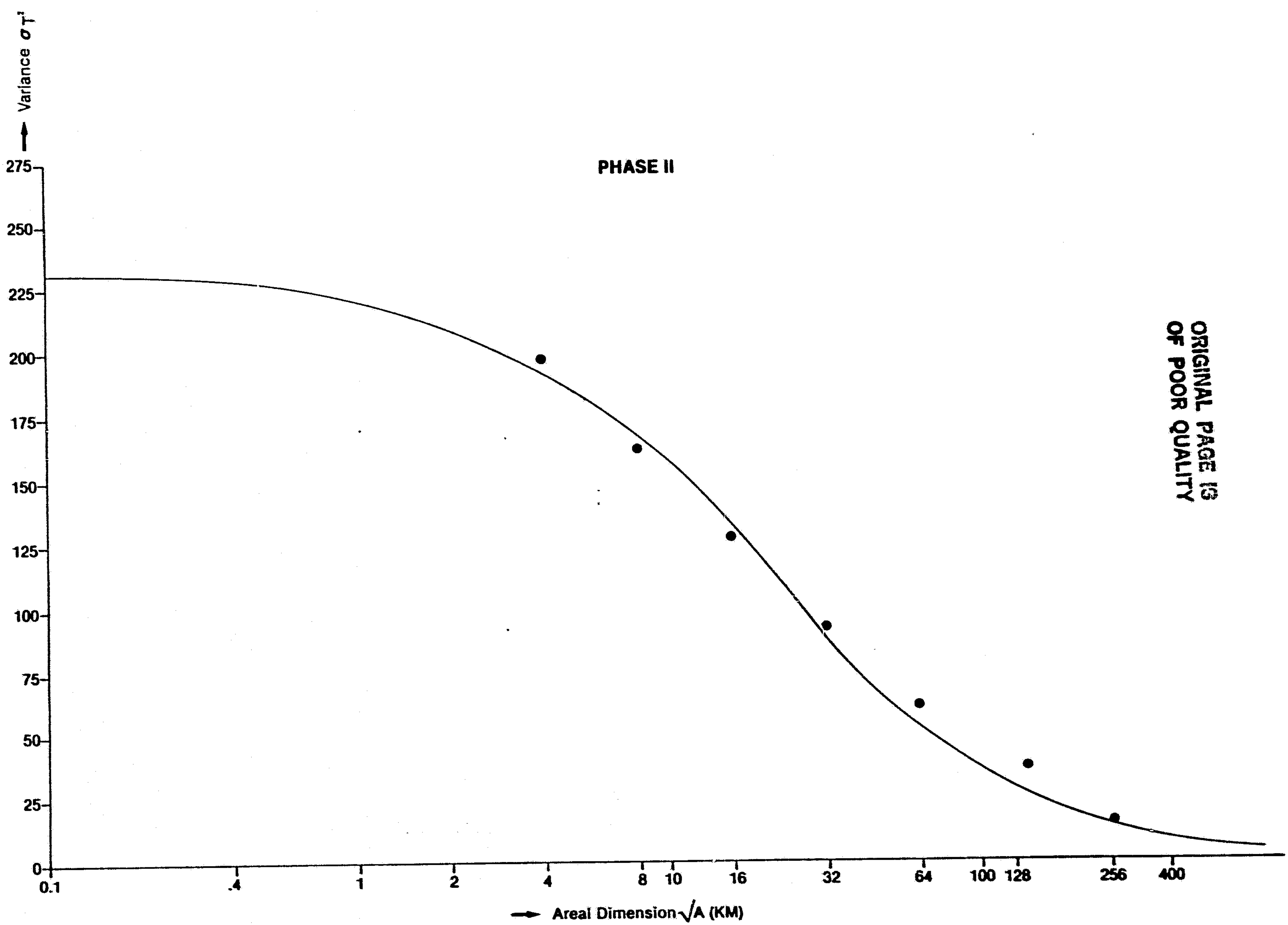

Figure 5-6

Variance σ_T^2 vs. Areal Dimension

TABLE 5-3

RESULTS FROM PARAMETER ESTIMATION TECHNIQUE

Phase	Population Variance	Spatial Correlation	Unbiased Estimate of Mean Rainfall
I	310	10	0.656
II	230	8	0.481

TABLE 5-4

RESULTS FROM ALTERNATE APPROACH

Phase	Population Variance	Spatial Correlation	Unbiased Estimate of Mean Rainfall
I	308	9	0.641
II	226	7.3	0.462

same time, there are no potentially significant gains to be made by using an antenna having a resolution of less than 1km or so.

To test the performance of parameter estimation technique, all computed values of σ_T^2 were used to find corresponding estimates of mean rainfall at various antenna resolutions. The results are shown in Figures 5-7 through 5-10 which show the behavior of mean rainfall, $\hat{R}$, corresponding variance, σ_R^2, and standard deviation, σ_R. This was done for both Phases I and II. The parameter estimation technique worked exceedingly well and, in addition, it was found that $\hat{R}$, σ_R^2 and σ_R all follow the functional form of equation 5.1 rather closely.

Error bounds on the estimate of population variance, σ_x^2, as obtained by evaluating equation (4.19) for six and twelve hour sampling rates are shown in Figures 5-11 and 5-12 for Phases I and II, respectively. These bounds are for 99% confidence level. Error bounds for one sigma confidence level were used to compute mean error (expressed as percentage of true mean rainfall) in estimating mean rainfall for various antenna resolutions. This was done for three measurement periods: 1 week, 2 weeks, and 1 month. The results are displayed in Figures 5-13 and 5-14 for Phases I and II, respectively. As expected the mean error increases as the radiometer antenna resolution decreases, i.e., as the physical size the antenna is decreased. For example, an antenna having a resolution of 8km results in mean error of approximately 3 percent of monthly mean with two observations per day as compared to approximately 6 percent mean error for an antenna having a resolution of 32km.

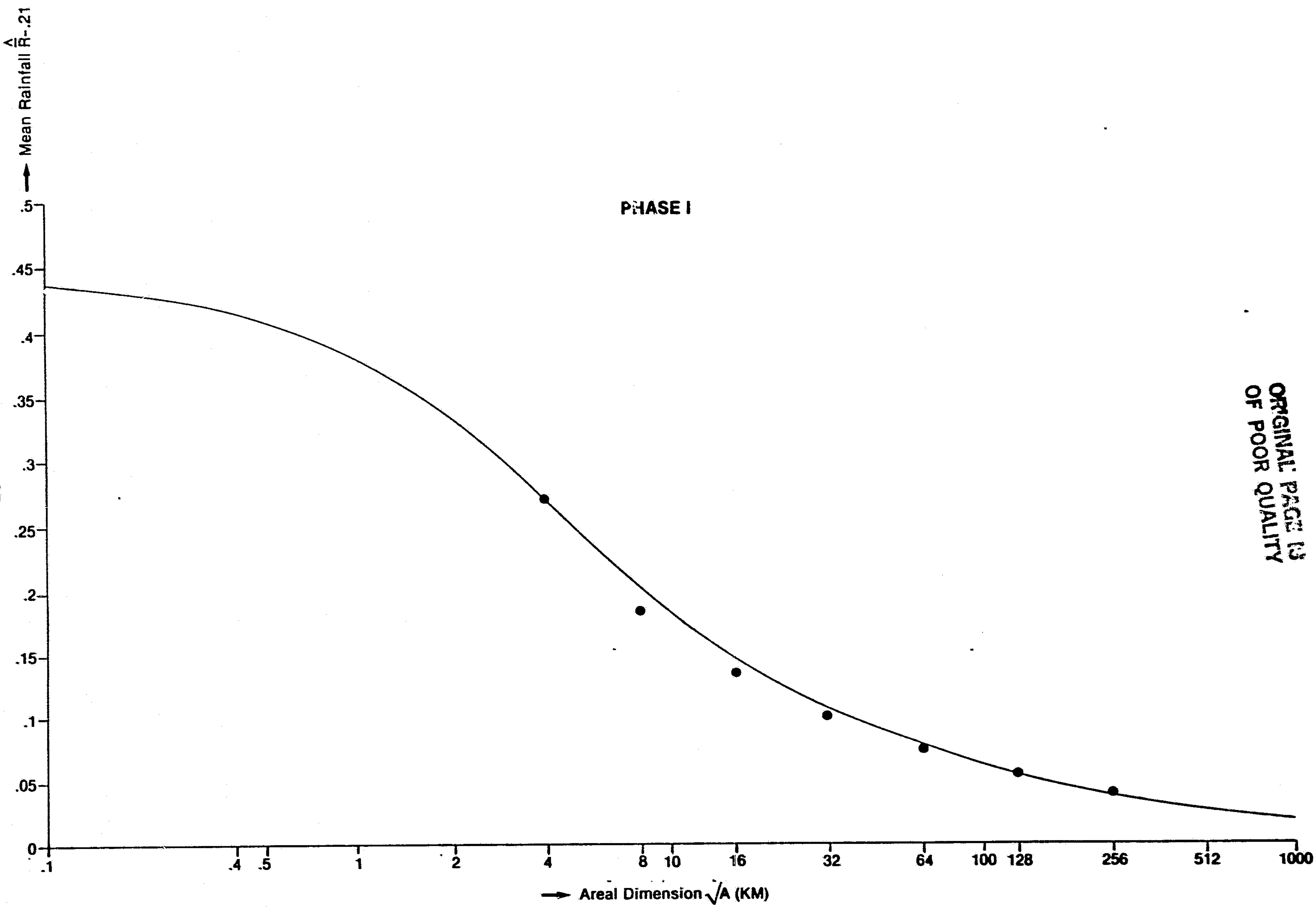

ORIGINAL PAGE IS
OF POOR QUALITY

Figure 5-7

Estimated Mean Rainfall $\hat{\bar{R}}$ vs. Areal Dimension

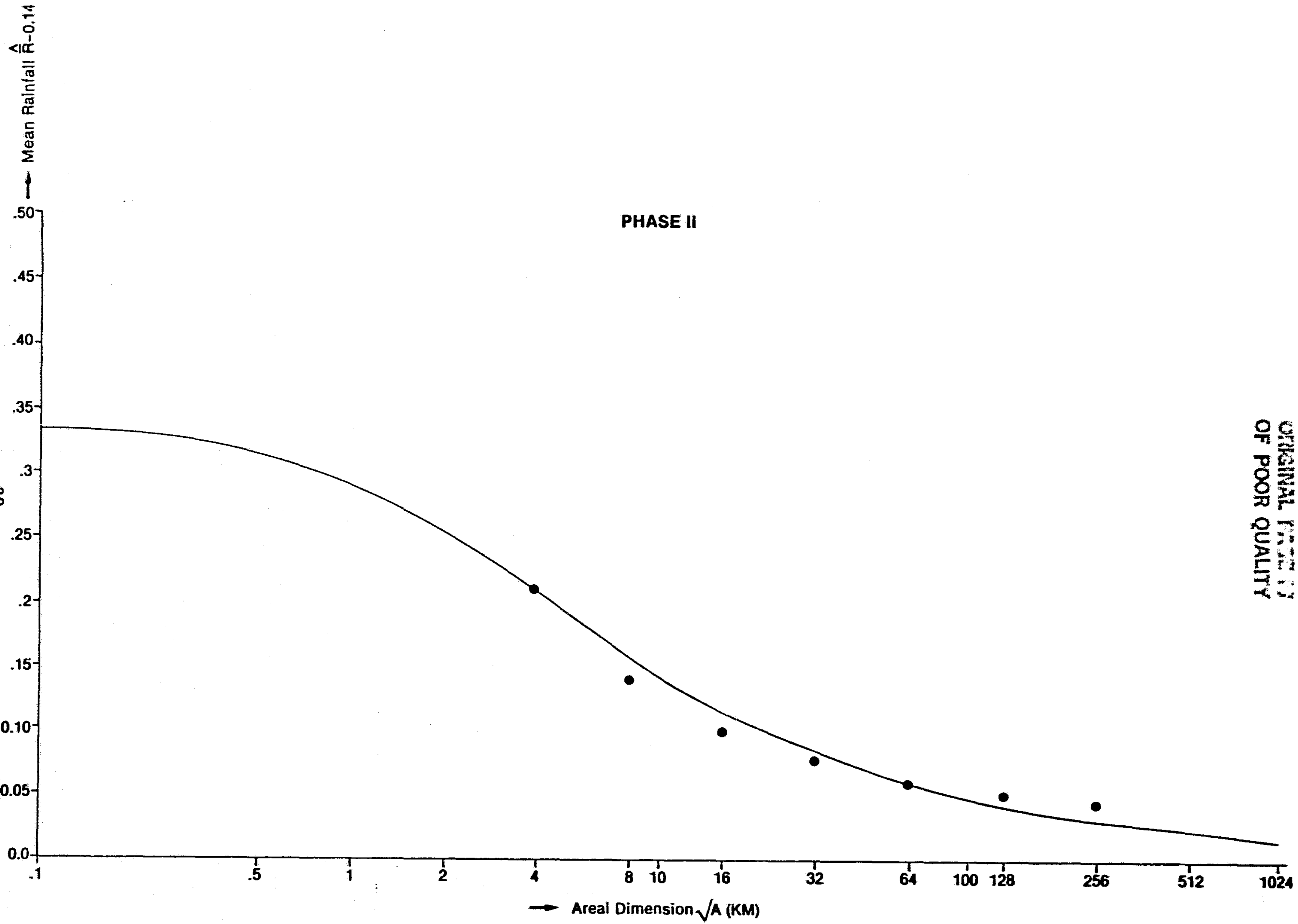

Figure 5-8

Estimated Mean Rainfall $\hat{\bar{R}}$ vs. Areal Dimension

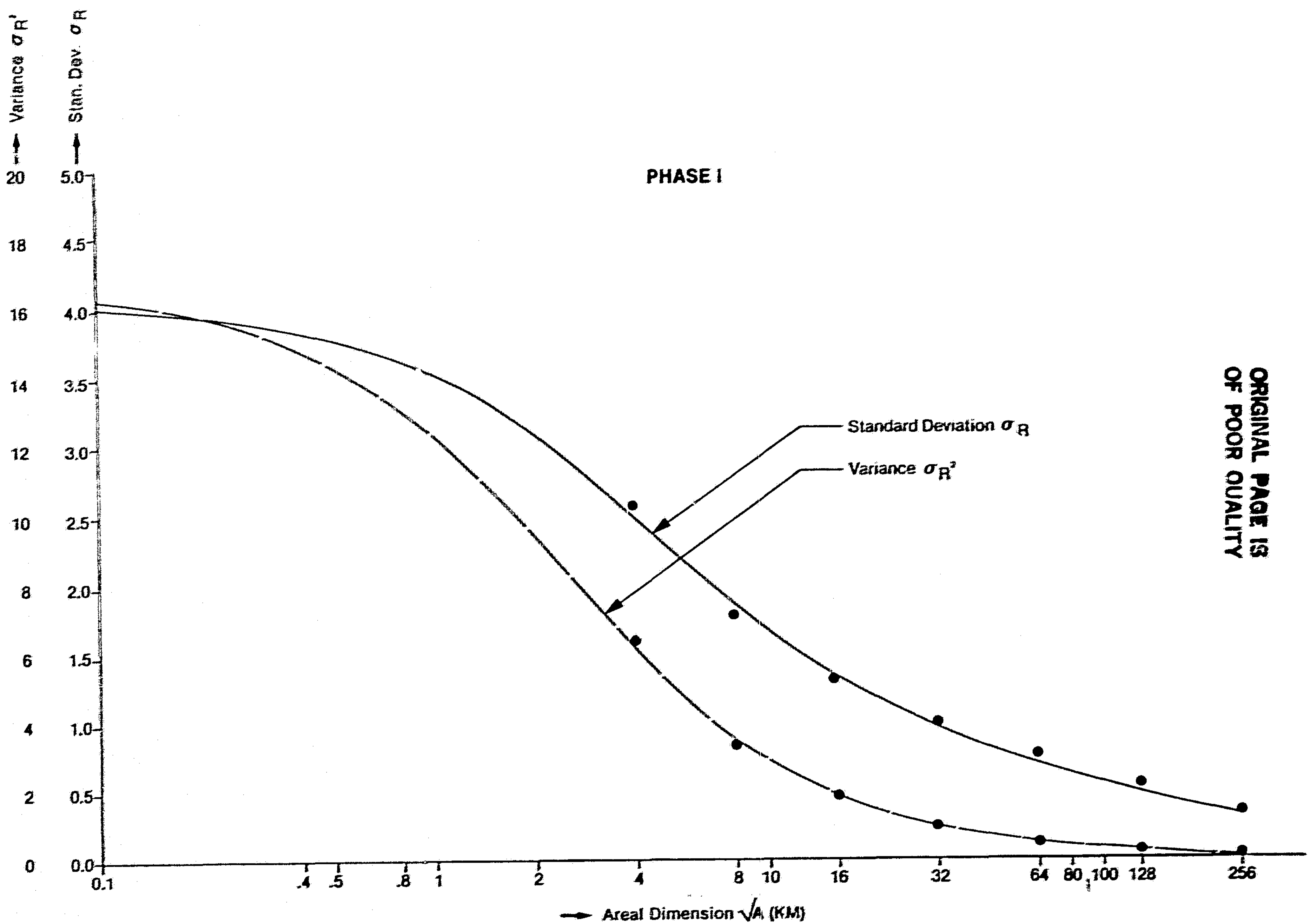

Figure 5-9
Variance σ_R^2 and Standard Deviation σ_R vs. Areal Dimension

ORIGINAL PAGE IS
OF POOR QUALITY

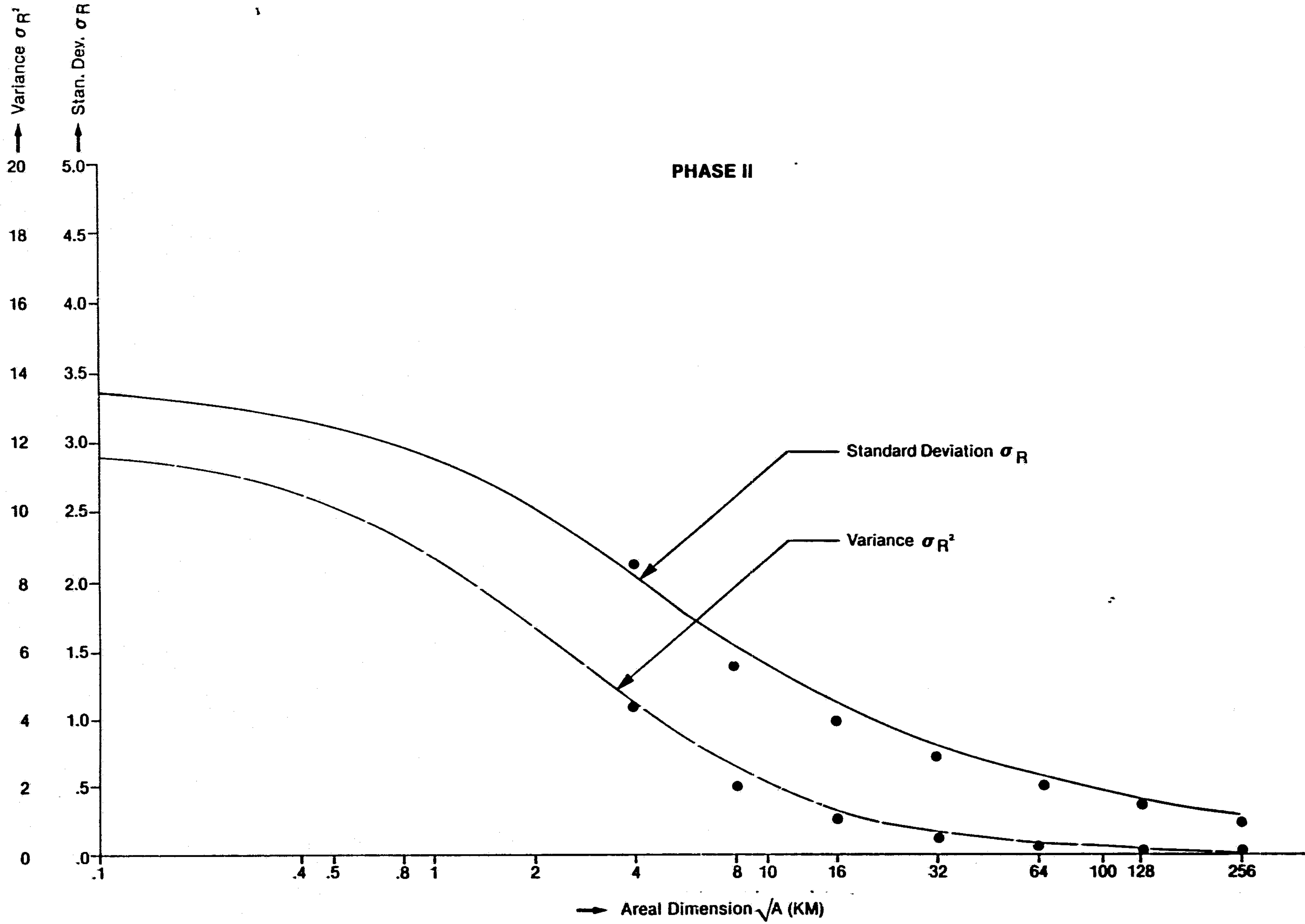

Figure 5-10
Variance σ_R^2 and Standards Deviation σ_R vs. Areal Dimension

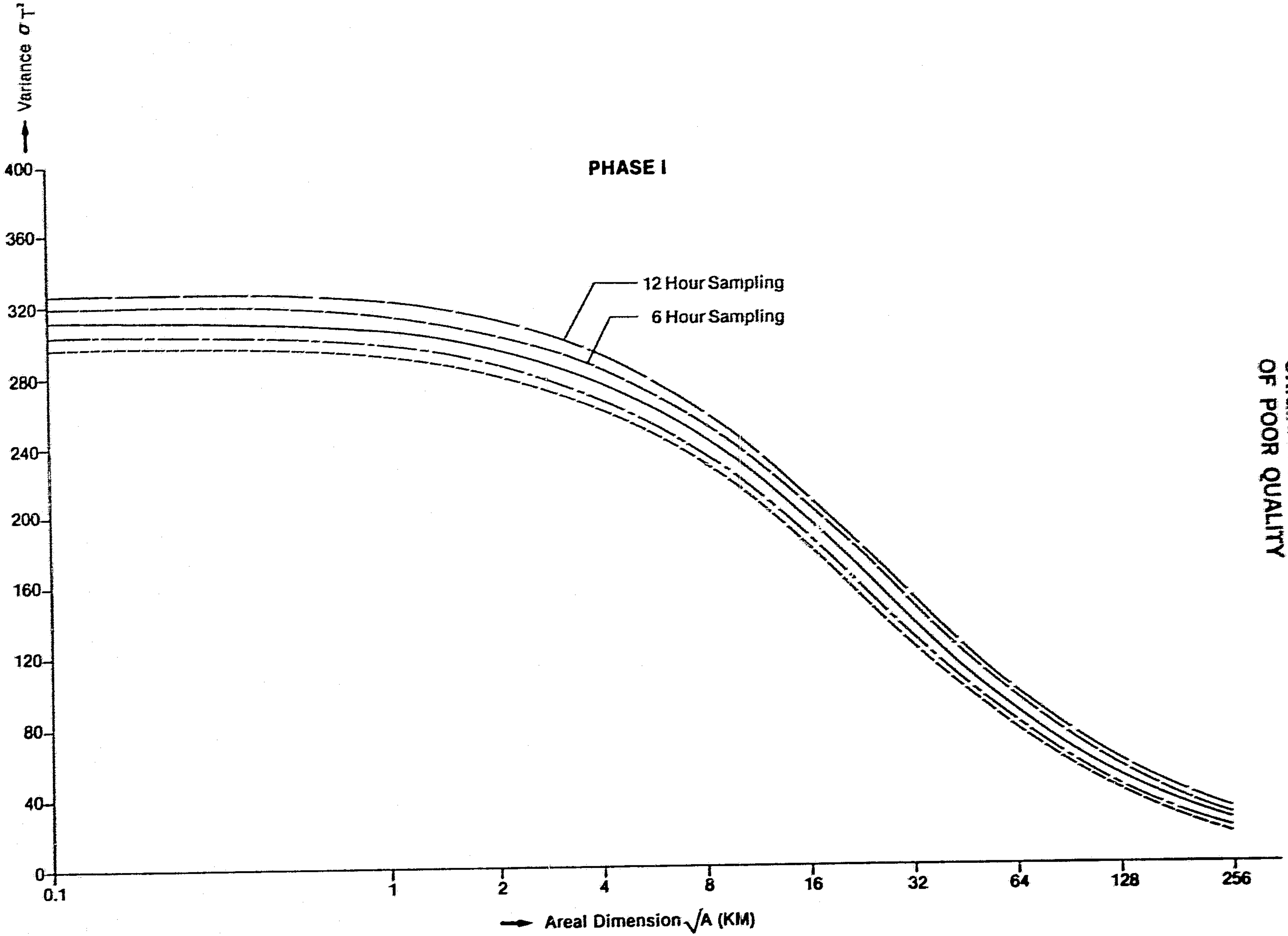

ORIGINAL PAGE IS
OF POOR QUALITY

Figure 5-11
Error Bounds on σ_T^2 for Six and Twelve Hour Sampling Rates vs. Areal Dimension

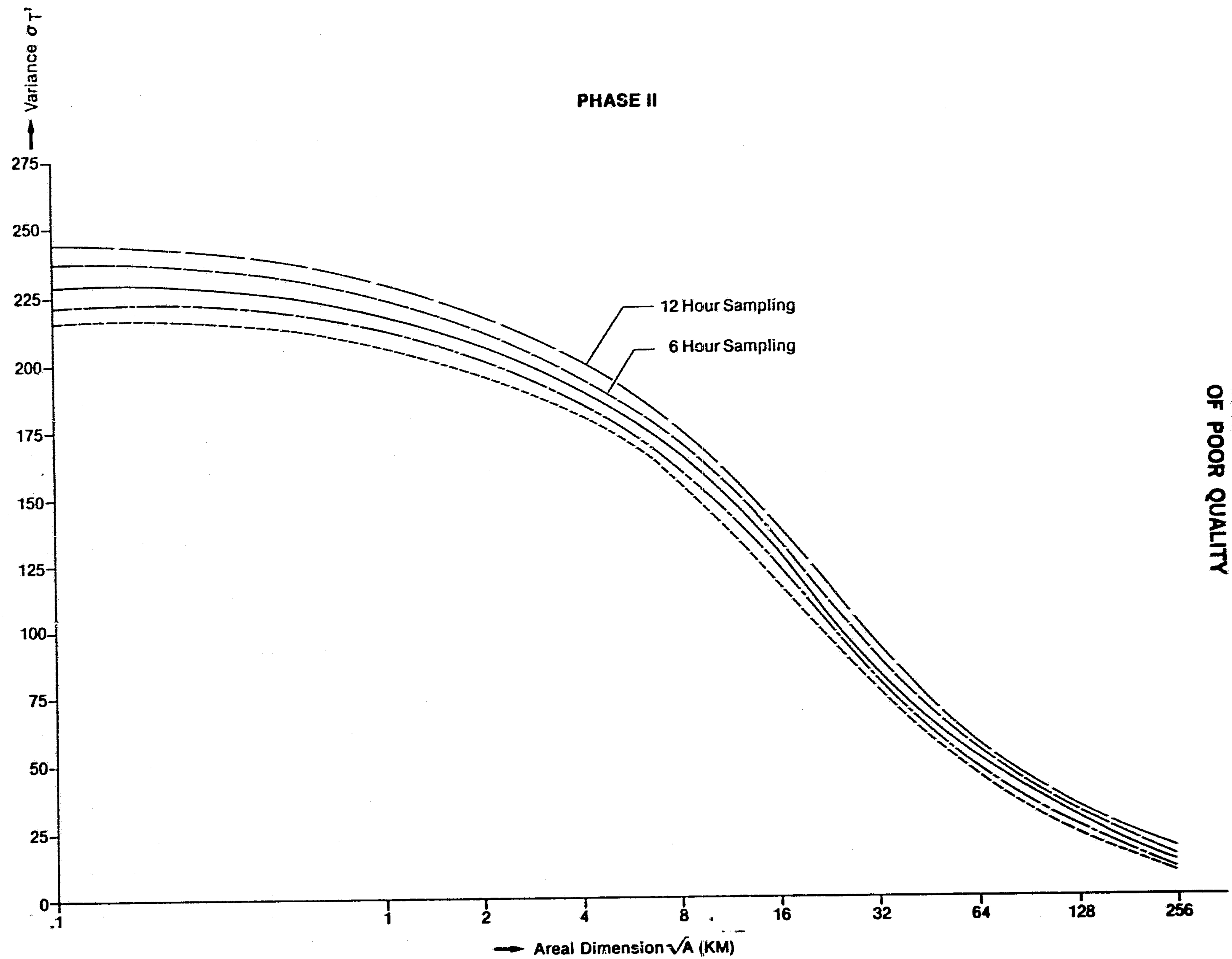

ORIGINAL PAGE IS
OF POOR QUALITY

Figure 5-12
Error Bounds on σ_T^2 for Six and Twelve Hour Sampling Rates vs. Areal Dimension

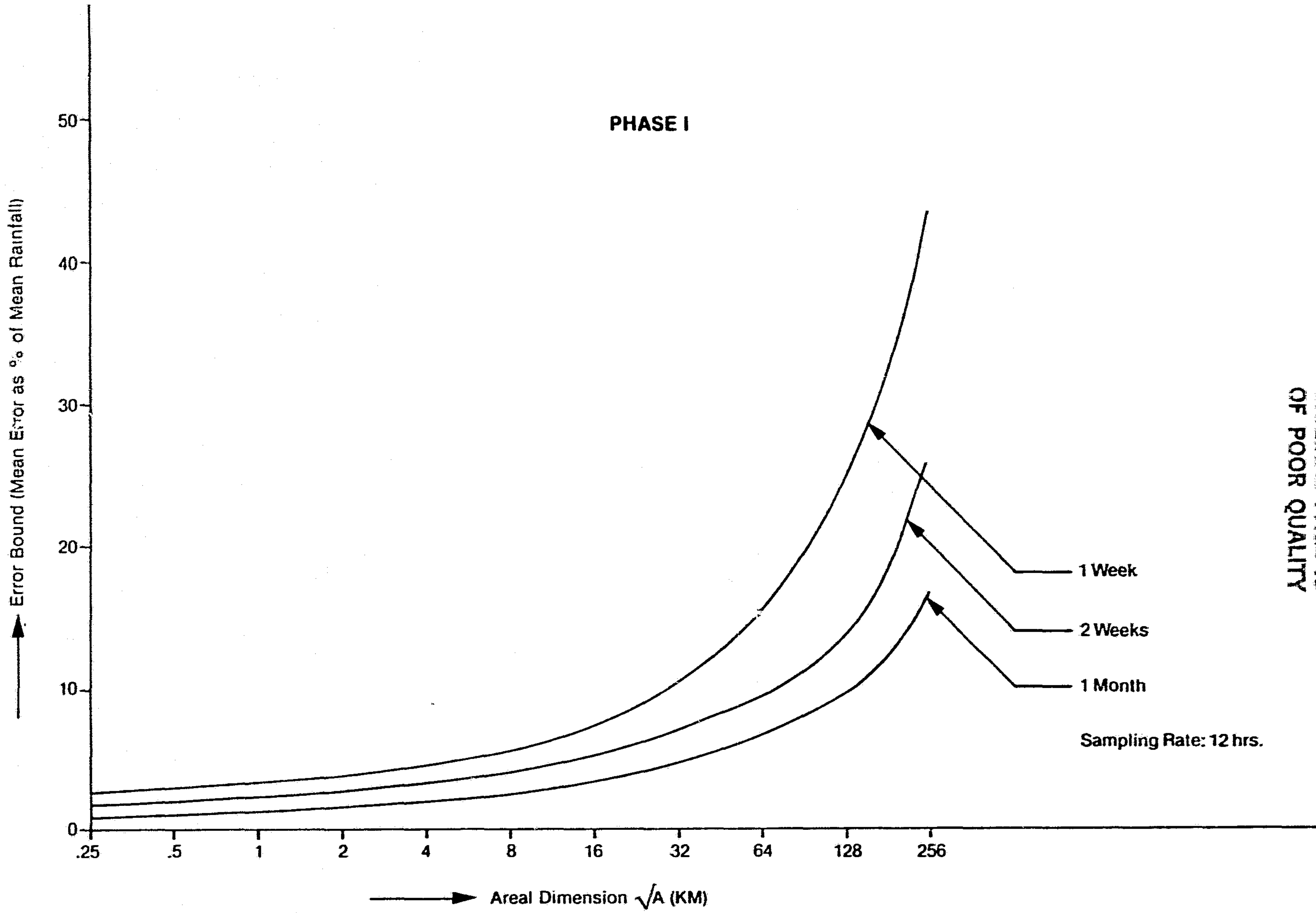

Figure 5-13
Error Bound (Mean Error as % of Mean Rainfall) vs. Antenna Resolution

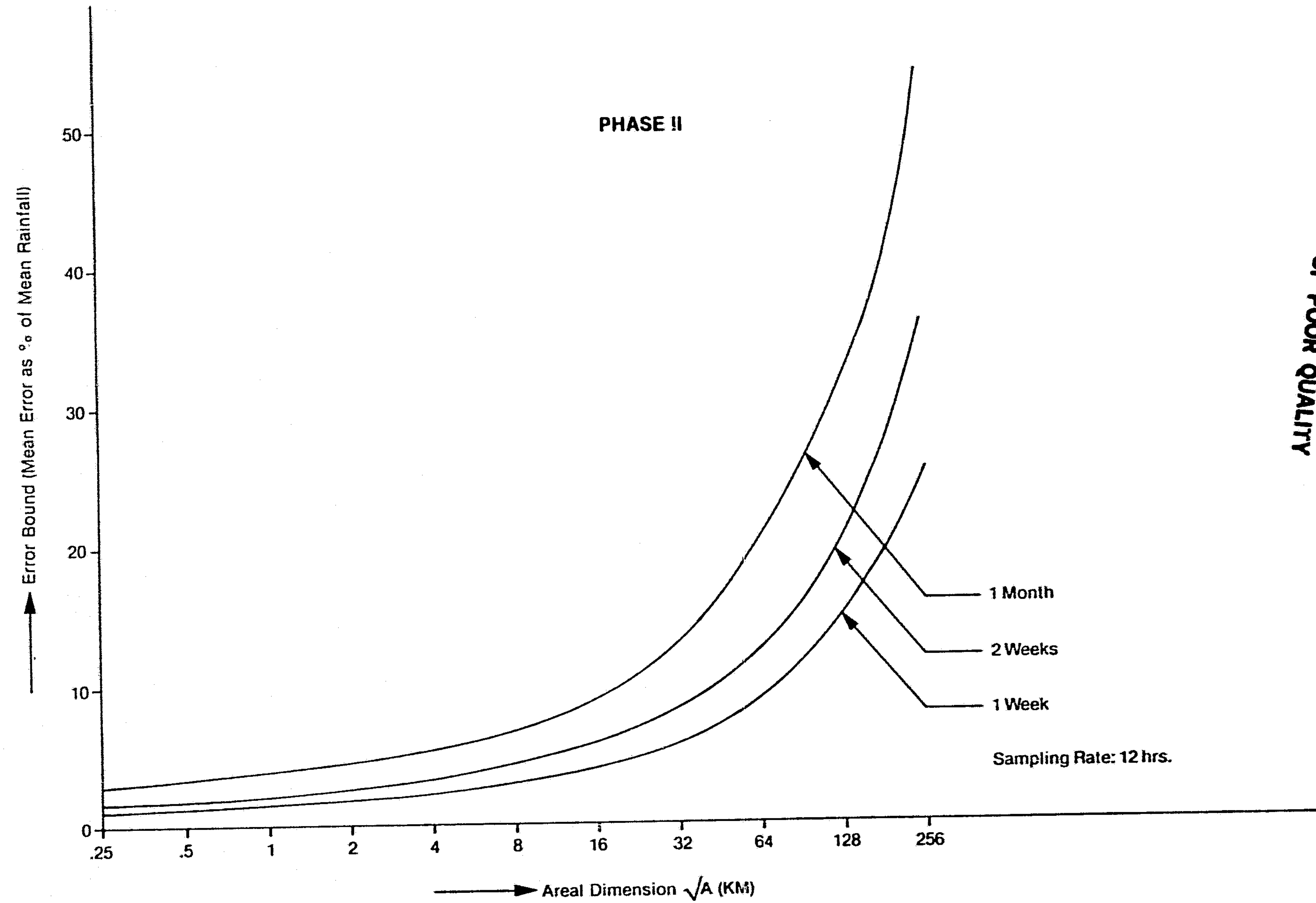

Figure 5-14
Error Bound (Mean Error as % of Mean Rainfall) vs. Antenna Resolution

The alternate approach developed in subsection 4.3 was tested and the preliminary results are fairly consistent with the results above. The correlation distance, D_o, was found to be 9km for Phase I and 7.3km for Phase II. These results are summarized in Table 5.4. This approach should be investigated further.

6.0 SUMMARY

The results of this work indicate that in order to obtain useful and unbiased estimates of monthly mean rainfall rate, an ESMR like instrument should be flown simultaneously on more than one satelite such that the effective re-visit time is approximately 6 hours. In addition, the resolution of the antenna should be consistent with the spatial correlation or correlation distance. The choice of antenna resolution of approximately 8 kilometers for radiometers of future such as LAMMR* agrees quite closely with the spatial correlation of about 8 kilometers as found by this study.

The bias due to non-uniform and incomplete filling of radiometer beamwidth can be eliminated with reasonably high confidence by using the proposed technique. The unbiased estimate of mean rainfall rate over the GATE area was found to be approximately 35 percent above the radar measurements. Also, the magnitude of error due to nonuniqueness of brightness temperature-rain rate relationship has been identified and found to be approximately 6 percent of the unbiased estimate of true mean rainfall.

---

* Large Aperture Multi-channel Microwave Radiometer

REFERENCES

Austin, P.M., Geotis, S., 1978: Evaluation of the Quality of Precipitation Data From a Satellite-Borne Radiometer, Report under NASA Grant NSG-5024, Department of Meteorology, Mass. Institute of Technology, Cambridge.

Davenport, W.B., Root, W.L., 1958: An Introduction to Theory of Random Signals and Noise, McGraw-Hill Book Co., Inc.

Hudlow, M., Patterson, V., 1979: GATE Radar Rainfall Atlas, NOAA Special Report, NOAA, U.S. Department of Commerce, Washington, D.C.

Laughlin, C.R., Gupta, J.N., 1980: Estimation of Rainfall From Sample Observations. To be published in Monthly Weather Review.

Papoulis, A., 1965: Probability, Random Variables and Stochastic Processes, McGraw-Hill Book Co., Inc.

Wilheit, T.T., et. al., 1977: A Satellite Technique for Quantitatively Mapping Rainfall Rates Over the Oceans, Journal of Applied Meteorology, Vol. 16, p. 551.

APPENDIX A

ORIGINAL PAGE IS
OF POOR QUALITY

APPENDIX A

Derivation of Equation (4.7)

From equation (4.6), mean brightness temperature, $\bar{T}$, is expressable as

$$\bar{T} = \int_0^{20} F(R)\ f_R(R,\alpha_R,\beta_R)\ dR \qquad (A.1)$$

Substituting for F(R) and $f_R(R,\alpha_R,\beta_R)$, one gets

$$\bar{T} = \int_0^{20} \left(a - b\ e^{-cR}\right) \frac{\beta_R^{\alpha_R}}{\Gamma(\alpha_R)}\ e^{-(\beta_R R)}\ R^{(\alpha_R-1)}\ dR$$

$$= a \int_0^{20} \frac{\beta_R^{\alpha_R}}{\Gamma(\alpha_R)}\ e^{-(\beta_R R)}\ R^{(\alpha_R-1)}\ dR \qquad (A.2)$$

$$- b \int_0^{20} \frac{\beta_R^{\alpha_R}}{\Gamma(\alpha_R)}\ e^{-(\beta_R+c)R}\ R^{(\alpha_R-1)}\ dR$$

Now, using the fact that

$$\int_0^{\infty} f_R(R,\alpha_R,\beta_R)\ dR = 1$$

we get,

$$\int_0^{20} e^{-(\beta_R R)}\ R^{(\alpha_R-1)}\ dR = \frac{\Gamma(\alpha_R)}{\beta_R^{\alpha_R}} \qquad (A.3)$$

ORIGINAL PAGE IS
OF POOR QUALITY

Therefore, from equations (A.2) and (A.3), $\bar{T}$, becomes

$$\bar{T} = a - b \frac{\beta_R^{\alpha_R}}{\Gamma(\alpha_R)} \frac{\Gamma(\alpha_R)}{(\beta_R+c)} \alpha_R$$

or

$$\bar{T} = a - b \frac{\beta_R^{\alpha_R}}{(\beta_R+c)^{\alpha_R}} \tag{A.4}$$

This completes the derivation of equation (4.7)

Derivation of Equations (4.9) and (4.10)

From Equation (4.8),

$$E\ [T_B^2] = \int_0^\infty T_B^2\ f_T\ (T_B,\alpha_T,\beta_T)\ dT$$

Substituting $T_B=F(R)$ from equation (4.2) and for $f_T(T_B,\alpha_T,\beta_T)$ from equation (4.3), we get

$$E\ [T_B^2] = \int_0^{20} (a - b\ e^{-cR})^2\ \frac{f_R(R,\alpha_R,\beta_R)}{F'(R)}\ F'(R)\ dR$$

$$= a^2 \int_0^{20} \frac{\beta_R^{\alpha_R}}{\Gamma(\alpha_R)}\ e^{-(\beta_R R)}\ R^{(\alpha_R-1)}\ dR$$

$$- 2ab \int_0^{20} \frac{\beta_R^{\alpha_R}}{\Gamma(\alpha_R)}\ e^{-(\beta_R+c)R}\ R^{(\alpha_R-1)}\ dR$$

$$+ b^2 \int_0^{20} \frac{\beta_R^{\alpha_R}}{\Gamma(\alpha_R)}\ e^{-(\beta_R+2c)R}\ dR$$

ORIGINAL PAGE IS
OF POOR QUALITY

Now using equation (A.3) and simplifying, this becomes

$$E\,[T_B^{\,2}] = a^2 - 2ab\left(\frac{\beta_R}{\beta_R+c}\right)^{\alpha_R} + b^2\left(\frac{\beta_R}{\beta_R+2c}\right)^{\alpha_R} \qquad (A.5)$$

Which is the same as equation (4.9).

Now, variance, $\sigma_T^{\,2}$, can be expressed as $\sigma_T^{\,2} = E[T_B^{\,2}] - \bar{T}^2$

Substituting for the two terms on right and simplifying,

$$\sigma_T^{\,2} = \left\{a^2 - 2ab\left(\frac{\beta_R}{\beta_R+c}\right)^{\alpha_R} + b^2\left(\frac{\beta_R}{\beta_R+2c}\right)^{\alpha_R}\right\}$$

$$-\left\{a^2 + b^2\left(\frac{\beta_R}{\beta_R+c}\right)^{2\alpha_R} - 2ab\left(\frac{\beta_R}{\beta_R+c}\right)^{\alpha_R}\right\}$$

$$\sigma_T^{\,2} = b^2\left(\frac{\beta_R}{\beta_R+2c}\right)^{\alpha_R} - \left(\frac{\beta_R}{\beta_R+c}\right)^{2\alpha_R} \qquad (A.6)$$

Which is the same as equation (4.10).

Further simplifications to the above equations are presented below. From equation (A.4),

$$\left(\frac{\beta_R}{\beta_R+c}\right)^{\alpha_R} = \frac{a-\bar{T}}{b}$$

or,

$$\alpha_R\,\ell n\left(\frac{\beta_R}{\beta_R+c}\right) = \ell n\left(\frac{a-\bar{T}}{b}\right)$$

or,

$$\alpha_R = \frac{L_1}{[\ell n\beta_R - \ell n(\beta_R+c)]} \qquad (A.7)$$

ORIGINAL PAGE IS
OF POOR QUALITY

Again, from equation (A.4), $b \frac{\beta_R}{\beta_R+c} = a - \bar{T}$ which when substituted in equation (A.6) results in,

$$\frac{\sigma_T^2}{(a-\bar{T})^2} + 1 = \frac{(\beta_R+c)^{2\alpha_R}}{\beta_R^{\alpha_R} (\beta_R+2c)^{\alpha_R}}$$

or,

$$\ell n \left(\frac{\sigma_T^2}{(a-\bar{T})^2} + 1 \right) = \alpha_R \left[2\ell n\ (\beta_R+c) - \ell n\beta_R - \ell n\ (\beta'_R+2c) \right] .$$

Substituting for α_R from equation (A.7) and letting $\ell n\left(\frac{\sigma_T^2}{(a-\bar{T})^2}+1\right) = L_2$ and simplifying, we get

$$L_2 = L_1 \frac{\left[2\ell n(\beta_R+c) - \ell n\beta_R - \ell n(\beta_R+2c) \right]}{\left[\ell n\beta_R - \ell n(\beta_R+c) \right]}$$

or,

$$\left(L_2 + 2L_1\right) \ell n\left(\beta_R+c\right) - \left(L_1 + L_2\right) \ell n\beta_R - L_1 \ell n\left(\beta_R+2c\right) = 0$$

or,

$$\ell n \left[\frac{(\beta_R+c)^{(L_2 + 2L_1)}}{\beta_R^{(L_1 + L_2)} \left(\beta_R+2c\right)^{L_1}} \right] = 0$$

or,

$$\frac{\left(\beta_R+c\right)^{(L_2 + 2L_1)}}{\beta_R^{(L_1 + L_2)} \left(\beta_R+2c\right)^{L_1}} = 1$$

or,

$$\left(\beta_R+c\right)^{(L_2 + 2L_1)} - \beta_R^{(L_2 + L_1)} \left(\beta_R+2c\right)^{L_1} = 0 \qquad \text{(A.8)}$$

which is the same as equation (4.12).

APPENDIX B

APPENDIX B

Derivation of Equation (4.18)

Equation (4.17) expresses $\sigma_T^2\ (D_a)$ as in (B.1)

$$\sigma_T^2\ (D_a) = \frac{2}{D_a} \int_0^{D_a} \left(1 - \frac{D'}{D_a}\right) R_x\ (D')\ \ dD' \qquad \text{(B.1)}$$

using, $R_x(D') = \sigma_x^2\ e^{-|D'|/D_o}$, one gets

$$\sigma_T^2\ (D_a) = \frac{2\sigma_x^2}{D_a} \int_0^{D_a} \left(1 - \frac{D'}{D_a}\right) e^{-|D'|/D_o}\ \ dD' \qquad \text{(B.2)}$$

The integrals involved in equation (B.2) can be easily evaluated to result in the following

$$\int_0^{D_a} D'\ \ e^{-|D'|/D_o}\ \ dD' = D_o^2 \left(1 - e^{-D_a/D_o}\right) - D_a\ D_o\ e^{-D_a/D_o}$$

and,

$$\int_0^{D_a} e^{-|D'|/D_o}\ \ dD' = D_o \left(1 - e^{-D_a/D_o}\right)$$

Substituting these in equation (B.2) and letting $\frac{D_a}{D_o} = y$

$$\sigma_T^2(D_a) = \frac{2\sigma_x^2}{D_a} \left[D_o(1-e^{-y}) - \frac{1}{D_a} \left| D_o^2\ (1-e^{-y}) - D_a\ D_o\ e^{-y} \right| \right]$$

$$= \frac{2\sigma_x^2}{D_a} \left[D_o - \frac{D_o^2}{D_a}\ \ (1 - e^{-y}) \right]$$

or,

$$\sigma_T^2 (D_a) = 2\sigma_x^2 \left[\frac{D_o}{D_a} - \frac{D_o^2}{D_a^2} (1 - e^{-y})\right]$$

or,

$$\sigma_T^2 (D_a) = 2\sigma_x^2 \left[\frac{1}{y} + \frac{1}{y^2} (-1 + e^{-y})\right] \qquad (B.3)$$

This completes the derivation. Further, in order to find the limiting value of $\sigma_T^2 (D_a)$ as D_a approaches 0, some further simplification of (B.3) is necessary as shown below. Also, L'Hospital's rule is used twice.

$$\lim_{D_a \to 0} \sigma_T^2 (D_a) = \lim_{y \to 0} 2\sigma_x^2 \left[\frac{y + (-1 + e^{-y})}{y^2}\right]$$

$$= \lim_{y \to 0} 2\sigma_x^2 \left[\frac{1 - e^{-y}}{2y}\right]$$

$$= \lim_{y \to 0} 2\sigma_x^2 \left[\frac{e^{-y}}{2}\right]$$

$$= 2\sigma_x^2 \left[\frac{1}{2}\right]$$

$$= \sigma_x^2$$

That is, as the averaging distance becomes smaller and smaller, $\sigma_T^2 (D_a)$ approaches σ_x^2, the population variance.

APPENDIX C

APPENDIX C

Numerical Method to Estimate σ_x^2 and D_o

Let σ_1^2 and σ_2^2 be the calculated values of σ_T^2 for averaging distances D_1 and D_2, respectively. Further, let $D_2 = 2D_1$ for sake of simplicity. Then substituting these values in equation (4.18), one gets

$$\sigma_1^2 = 2B\left[\frac{D_o}{D_1} + \left(\frac{D_o}{D_1}\right)^2 \left(-1 + e^{-D_1/D_o}\right)\right] \tag{C.1}$$

and,

$$\sigma_2^2 = 2B\left[\frac{D_o}{2D_1} + \left(\frac{D_o}{2D_1}\right)^2 \left(-1 + e^{-2D_1/D_o}\right)\right] \tag{C.2}$$

Dividing equation (C.1) by (C.2) and letting $\dfrac{\sigma_1^2}{\sigma_2^2} = k$ results in the following,

$$\frac{4\left[D_1 + D_o\left(-1 + e^{-D_1/D_o}\right)\right]}{\left[2D_1 + D_o\left(-1 + e^{-2D_1/D_o}\right)\right]} = k \tag{C.3}$$

Let,

$$Z = e^{-D_1/D_o} \tag{C.4}$$

Now, noting that $(-1 + Z^2) = (Z-1)\,(Z+1)$, equation (C.3) becomes

$$\frac{4\,[\ell nZ - (Z-1)]}{[2\ell nZ - (Z-1)\,(Z+1)]} = k$$

or,

$$(4 - 2k)\,\ell nZ - 4Z + kZ^2 + (4 - k) = 0 \tag{C.5}$$

Equation (C.5) is solved numerically for Z. The correlation distance, D_o, is then obtained from equation (C.4) as

$$D_o = -\frac{D_1}{\ell n Z}$$

Substituting this D_o in either equation (C.1) or equation (C.3) will provide appropriate value of B.